NEUROSCIENCE of Consciousness

Neuroscience of Consciousness, 2025, **2025(1)**, niaf055

DOI: https://doi.org/10.1093/nconsc/niaf055

Research Article

Neural field modeling and analysis of consciousness states in the brain

Daniel Polyakov [1,*], P.A. Robinson[2], Avigail Makbili[1], Steven Laureys[3,4,5], Olivia Gosseries[3,4,†], Oren Shriki[1,†]

[1]Department of Cognitive and Brain Sciences, Ben-Gurion University of the Negev, David Ben Gurion Blvd 1, Be'er-Sheva 8410501, Israel
[2]School of Physics, The University of Sydney, Sydney, NSW 2006, Australia
[3]Coma Science Group, GIGA Consciousness, University of Liège, Avenue de l'Hopital 1, 4000, Liège, Belgium
[4]NeuroRehab & Consciousness Clinic, Neurology Department, University Hospital of Liège, Avenue de l'Hopital 1, 4000, Liège, Belgium
[5]Joint International Research Unit on Consciousness, CERVO Brain Research Centre, Laval University, 2601 de la Canardière, G1J 2G3, Québec, Canada
*Corresponding author. David Ben Gurion Blvd 1, Be'er Sheva 8410501, Israel. E-mail: danpol@gmail.com
†These authors contributed equally to this work.

Abstract

Understanding the neural correlates of consciousness remains a central challenge in neuroscience. In this study, we explore the potential of neural field theory (NFT) as a computational framework for representing consciousness states. While prior research has validated NFT's capacity to differentiate between normal and pathological states of consciousness, the relationship of its parameters to the representation of consciousness states remains unclear. Here, we fitted a corticothalamic NFT model to the electroencephalography (EEG) data collected from healthy individuals and patients with disorders of consciousness. We then comprehensively explored the correlations between the fitted NFT parameters and features extracted from both experimental and simulated EEG data across various states of consciousness. The identified correlations not only highlight the model's ability to differentiate between healthy and impaired states of consciousness, but also shed light on the physiological bases of these states, pinpointing potential biomarkers. Our results provide valuable insights into how consciousness levels are represented within the NFT framework and into the dynamics of brain activity across normal and pathological states of consciousness. This underscores the potential of NFT as a useful tool for consciousness research, facilitating *in-silico* experimentation.

Keywords: neural field theory; disorders of consciousness; neural correlates of consciousness; neural activity modeling; EEG

Introduction

Neural correlates of consciousness

Consciousness is a fascinating, hardly explained phenomenon. It exhibits a remarkable fluidity, transitioning in and out of our awareness throughout the day. We experience its return upon waking in the morning, or its decline when we become drowsy after a satisfying meal. At times, we find ourselves drifting into a dreamlike state during moments of daydreaming. Paradoxically, it can entirely dissipate during deep sleep and then resurface during the enigmatic realm of dreams. Moreover, consciousness is subject to the influence of various substances, such as anesthetics and psychedelics, which can either augment or diminish its presence. Furthermore, it can be substantially impaired by an array of brain lesions and diseases, resulting in disorders of consciousness (DoC), like coma or unresponsive wakefulness syndrome (UWS).

The study of consciousness has long captivated the imagination of philosophers, psychologists, and neuroscientists alike, igniting a profound quest to unravel the enigmatic neural underpinnings of this elusive phenomenon. This quest has given rise to an intriguing and multifaceted field of inquiry known as the "Neural Correlates of Consciousness" (NCC). The formation of the NCC field dates back approximately 30 years to the collaborative efforts of Nobel laureate Crick and Koch (1990), and it has since experienced tremendous growth. The NCC seeks to elucidate the intricate relationship between subjective experience and the activity of the brain, striving to identify the specific neural mechanisms that generate our awareness of the world. This burgeoning field not only enhances our understanding of consciousness, but also holds the potential to shed light on a wide range of cognitive and clinical phenomena, ranging from transcendental meditation to absence epileptic seizures, ultimately deepening our insight into the fundamental nature of human existence.

Among the various brain regions associated with consciousness, the corticothalamic system plays a central role. It is responsible for both the state and contents of consciousness by integrating sensory information, regulating attention, and enabling widespread neural communication across the brain. This system comprises reciprocal connections between the cortex and the thalamus, which are essential for maintaining wakefulness, perception, and cognitive functions (Koch and Tsuchiya, 2007, Tononi et al. 2016a, Boly et al., 2017, Darracq et al., 2018, Laufs et al., 2019,

Received 16 July 2025; **revised** 4 November 2025; **accepted** 14 November 2025

Pal et al., 2019, Sergent et al., 2021). The thalamus serves as an organizing hub, filtering and modulating sensory inputs before transmitting them to the cortex for higher-order processing—thereby shaping the contents of consciousness and gating their emergence. Additionally, corticothalamic loops support the synchronization of neural activity, a process often linked to conscious awareness. Transitions between conscious and unconscious states are mediated by matrix thalamic neurons, which modulate cortical excitability (Lau and Rosenthal, 2011, Koch et al., 2016, Tononi et al. 2016a, Sanchez-Vives et al., 2017, Muller et al., 2023, Whyte et al., 2024). Disruptions in this system—whether due to DoC, sleep, or anesthesia—result in impaired consciousness, underscoring its fundamental role (Brown et al., 2010, Vanhaudenhuyse et al., 2010, Gosseries et al., 2011, Darracq et al., 2018, Mashour and Hudetz, 2018, Mohanta et al., 2021). Research has shown that key consciousness-related processes, such as information integration and large-scale network coordination, depend on corticothalamic interactions (Tononi, 2008, Tononi et al. 2016b, Haun et al., 2017, Demertzi et al., 2019), making this system a key candidate for understanding the neural basis of consciousness.

Consciousness-level quantification

Quantifying the level of consciousness poses a significant challenge within the domains of neuroscience and cognitive science. A plethora of methods and features have been developed to capture and measure this intricate aspect of human experience. Researchers often rely on behavioral observations and subjective self-report assessments to evaluate levels of consciousness, considering factors such as responsiveness, memory, and self-awareness. Another approach involves electrophysiological analysis of the brain through electroencephalography (EEG), intending to identify specific neural activity signatures associated with distinct states of consciousness.

EEG-based biomarkers of consciousness states typically rely on either power spectra or time-series complexity. Metrics like power in different frequency bands vary across wakefulness, sleep, anesthesia, and DoC. For instance, Delta and Theta band power increase with loss of consciousness, while higher Alpha and Gamma power are typical in healthy wakeful states (Piarulli et al., 2016, Darracq et al., 2018, Bai et al., 2021). A more sophisticated metric is the spectral exponent β, or the spectral slope on a logarithmic scale, which is derived from the power law behavior of the EEG spectrum $P(f) \propto f^{-\beta}$, also termed "$1/f$ spectrum." Research indicates that this slope tends to be steeper during sleep and anesthesia compared to wakefulness in healthy participants (Freeman and Zhai, 2009, Colombo et al., 2019, Maschke et al., 2022, Medel et al., 2023). Spectral entropy, which estimates the complexity of the power spectrum, also holds promise for estimating consciousness states, with higher values typically observed in less severe DoC states (Piarulli et al., 2016, Martens et al., 2021). For assessing time-series complexity, Lempel-Ziv complexity (LZc) is commonly employed, measuring the rate at which unique patterns appear in brain activity. LZc analysis of resting-state EEG in neurotypical participants has proven capable of distinguishing between anesthetic, psychedelic, and wakeful states, with higher conscious states exhibiting greater EEG complexity (Schartner et al., 2017, Fekete et al., 2018, Li and Mashour, 2019, Medel et al., 2023). Moreover, LZc analysis of EEG signals acquired after transcranial magnetic stimulation has successfully differentiated among DoC states (Casali et al., 2013). Conversely, permutation entropy (PE) assesses the degree of disorder or randomness within the time series of neural signals. PE has been effectively utilized in epilepsy research and demonstrated the ability to discriminate between various sleep stages, with lower PE values corresponding to deeper sleep stages (Ouyang et al., 2013, Mateos et al., 2018).

Disorders of consciousness

DoC encompass a range of conditions characterized by impaired awareness and wakefulness resulting from severe brain damage. These conditions include coma, UWS, and minimally conscious state (MCS) (Gosseries et al., 2011). Coma is an acute state in which both wakefulness and awareness are absent. UWS corresponds to the recovery of wakefulness without signs of awareness, while MCS is defined by the presence of wakefulness with fluctuating but discernible signs of awareness, such as visual pursuit or localization to pain. Within the MCS category, patients are often further classified as MCS– or MCS+ based on their nonreflex responses, verbal abilities, and command following (Bruno et al., 2011). Collectively, these conditions disrupt the complex neural processes that underlie human consciousness irrespective of arousal, challenging our fundamental understanding of how the brain forms awareness, and cognition, thereby prompting profound scientific, clinical, and ethical inquiries (Bernat, 2006, Gosseries et al., 2011).

The term "emergence from MCS" (eMCS) refers to the condition when MCS patients regain functional communication or object use. Although eMCS patients often exhibit levels of awareness and responsiveness approaching those of healthy individuals, we include it in our study under the DoC umbrella. This choice is motivated by the fact that patients in eMCS continue to suffer from the consequences of earlier brain injuries that impaired consciousness (Giacino et al., 2004, Bodien et al., 2020).

In the present work, we analyze a dataset of patients with DoC (see the "Experimental data" section under Methods). This particular dataset is advantageous because it encompasses four distinct and clearly defined states of consciousness, ranging from the lowest level in UWS, progressing through MCS–, and MCS+, to the highest level of eMCS and healthy wakefulness. In contrast to binary conscious/unconscious datasets, a multi-level dataset offers the opportunity to test for more refined classification capabilities and provides a detailed interpretation of various DoC states. Additionally, it enables us to treat the consciousness level as an approximately continuous function, which is useful for conducting correlation analyses.

Brain activity model for consciousness representation

Over the past half-century, substantial progress has been made in the development of brain activity models, addressing a wide range of phenomena occurring across different brain regions and scales (Robinson et al., 2005, Markram, 2006, Sanz-Leon et al., 2013, Li et al., 2021). A significant focus of these efforts has been the creation of comprehensive, physiology-based, multiscale models that can simulate various brain phenomena and produce realistic signals. Finding such a model, that is capable of reliably representing different levels and states of consciousness can be very helpful in many research aspects in this field. Such a model would be immensely valuable for interpreting various phenomena, generating hypotheses, and conducting *in-silico* experiments. For instance, consider the scenario of designing a novel therapy for patients with DoC. First, we can fit the model to each individual patient with DoC, and the model's parameters can be explored to gain a deeper understanding of the physiological condition of each patient. Subsequently, a personalized therapy plan can be proposed for each patient, based on the state of their fitted model.

Following this, we can perform a simulation of the proposed therapy applied to the model, with the generated output signal serving as a tuning mechanism and a biomarker for the desired therapeutic effect (Polyakov et al., 2025). Only after a successful outcome in the virtual model can these strategies be cautiously extended to real-life patient trials. This approach minimizes risks and optimizes the potential for therapeutic success in a highly controlled and personalized manner.

A robust multiscale brain activity model for consciousness representation should ideally possess several key attributes. First, it should be versatile enough to capture and simulate a wide range of consciousness states, such as sleep, anesthesia, and epileptic seizures. Second, the model should have a physiologically grounded structure and dynamics, reliably reflecting neural processes across different spatial scales. Third, it should generate output data that closely resemble experimental recordings, such as EEG or local field potentials, serving as measurable manifestations of the modeled phenomena. Lastly, the model should be adaptable, allowing its parameters to be fitted to experimental data to represent individual subjects in specific consciousness states. These fitted parameters can provide valuable physiological insights, such as synaptic delays or firing rates. Importantly, both the fitting process and data generation should be computationally efficient, enabling practical research applications without excessive computational demands.

We have evaluated various models that hold the potential to fulfill this purpose. Among them, the most renowned is the "Blue Brain Project," which seeks to construct a precise cortical network by linking detailed single-neuron models with anatomically derived connections. However, the project has encountered computational limitations, particularly when attempting to simulate large neuronal populations, let alone the entire brain (Markram, 2006). A more pragmatic alternative is "The Virtual Brain," which represents brain regions through neural mass models (Wilson and Cowan, 1973, Jansen and Rit, 1995) that are interconnected based on connectome data. This model has the capability to simulate diverse phenomena such as epilepsy and sleep stages. Nonetheless, the challenge lies in fitting neural mass models to experimental data due to the utilization of non-linear differential equations to generate the activity of each region (Sanz-Leon et al., 2013, Wang et al., 2024). In contrast, neural field theory (NFT) modeling offers an efficient approach to constructing networks of interconnected brain regions that interact through wave equations. The NFT framework provides convenient tools for fitting and simulating neural activity, and EEG in particular, using standard computing equipment (Robinson et al., 2005, Abeysuriya et al., 2015, Sanz-Leon et al., 2018). Furthermore, the corticothalamic NFT model (CTM) has shown efficacy in representing various consciousness-related phenomena, such as sleep stages and epilepsy (Robinson et al., 2002, Breakspear et al., 2006, Abeysuriya and Robinson, 2016), and it has also been applied to classify DoC states (Assadzadeh et al., 2023). This makes NFT an attractive candidate for creating models that can deepen our understanding of consciousness and related disorders.

Research motivation

In this study, we aim to assess the potential of NFT modeling as a viable tool in the research of the NCC. Specifically, we focus on DoC, which are associated with large-scale alterations in awareness and arousal states. Given that the corticothalamic system plays a central role in mediating consciousness and generating EEG signals in healthy wakefulness (Tononi et al. 2016a, Boly et al., 2017, Muller et al., 2023), we employ the CTM, a framework extensively applied in consciousness-related research (Breakspear et al., 2006, Robinson et al., 2011, Abeysuriya and Robinson, 2016, Assadzadeh et al., 2023). While previous studies have suggested that NFT modeling can reproduce several consciousness-related phenomena, its ability to systematically reflect different states of consciousness in a physiologically meaningful way remains unclear. We hypothesize that the modeled state of consciousness correlates with fitted NFT parameters and EEG-based features, both experimental and simulated.

To test this, we exploit the ability of the CTM to be easily fitted to experimental EEG data and to, subsequently, generate artificial EEG signals accordingly (Rennie et al., 2002, Robinson et al., 2002, 2004, Rowe et al., 2004, O'Connor and Robinson, 2005, Kerr et al., 2008, Abeysuriya et al., 2015). We then extract a variety of features from both the experimental and simulated EEG data. This process is applied to a dataset comprising patients with DoC (UWS, MCS–, MCS+, eMCS) and healthy subjects, allowing us to explore correlations between these features, the model parameters, and different consciousness states. Additionally, we aim to show that fitted NFT parameters can be employed for the classification of consciousness states, as well as for their physiological interpretation. The parameters also offer insights into the interpretation of features based on simulated EEG that are correlated with them. The correlations observed between experimental-EEG-based and simulated-EEG-based features suggest that a fitted CTM can reproduce and control them.

Through our work, we not only replicate findings from prior research, but also furnish evidence supporting theoretical predictions and offering new theoretical insights into the NCC. Additionally, we unveil numerous new abilities and characteristics inherent to an NFT model. By systematically evaluating the CTM's capacity to model healthy and damaged brain states, this study helps bridge computational modeling and experimental neuroscience. The knowledge derived from our findings enables us to ascertain the capability of NFT to represent consciousness in the healthy and damaged brain, reinforcing its value as a tool for investigating this fascinating aspect of the human mind.

Materials and methods

Neural field theory

Neural-field modeling (Robinson et al., 2001, 2004, 2005) stands as a tool for constructing physiologically inspired brain models capable of mimicking various multiscale measures of brain activity. This approach captures a continuum of corticothalamic activity by simulating the local dynamics in each population and employing wave equations to describe the propagation between these populations (O'Connor and Robinson, 2004). Consequently, it effectively replicates and integrates numerous phenomena observed in EEG data, including spectral peaks observed during waking and sleeping states, event-related potentials, measures of connectivity, and spatiotemporal structure, and even the dynamics of epileptic seizures (see Fig. 1) (Rennie et al., 2002, Rowe et al., 2004, O'Connor and Robinson, 2005, Breakspear et al., 2006, Fulcher et al., 2008, Kerr et al., 2008, Nevado-Holgado et al., 2012, Robinson et al., 2014). The model's parameters encompass various biophysically meaningful quantities such as synaptic strengths, excitatory and inhibitory gains, propagation delays, synaptic and dendritic time constants, and axonal ranges. NFT represents a bottom-up approach to whole-brain modeling, which involves averaging over microstructure to derive mean-field equations. This method effectively complements analyses conducted at the cellular and local neural network levels. Additionally, NFT's

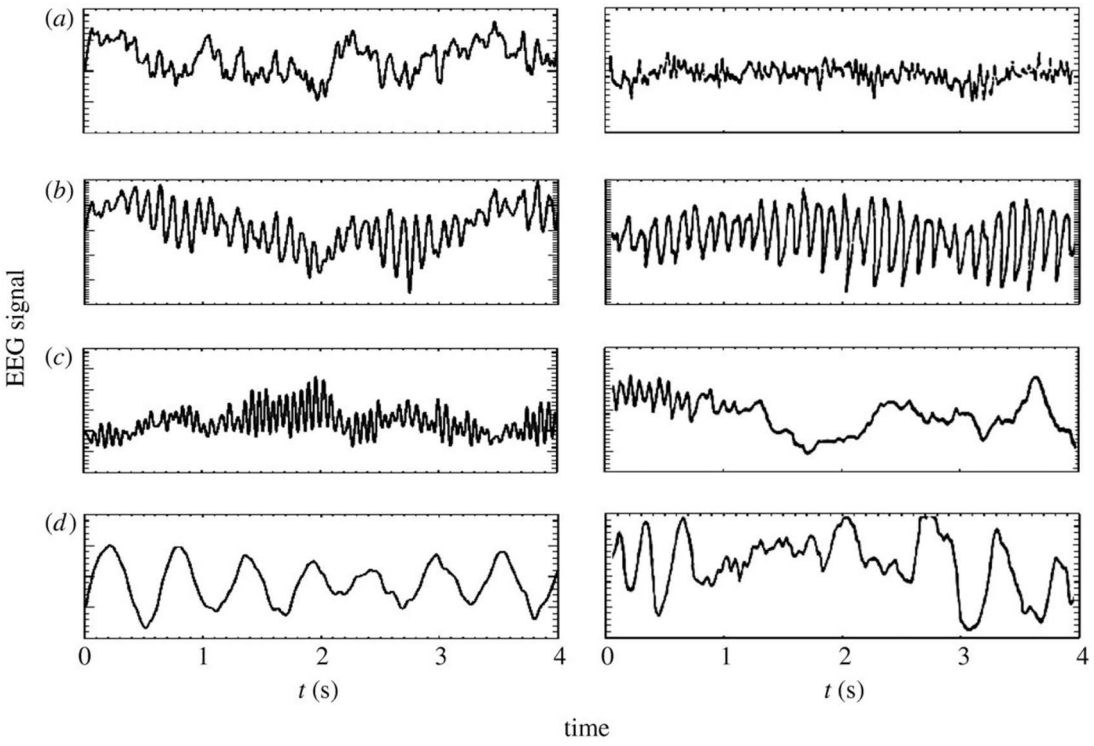

Figure 1. Simulated VS experimental EEG time series of waking and sleeping states. In the left panels: model generated time series of (a) eyes-open resting state, (b) eyes-closed resting state, (c) sleep-stage 2, and (d) sleep-stage 3. In the right panels: corresponding time series from human subjects. Penfield and Jasper (1954), Nunez (1995). (The figure was originally published by Robinson et al. (2005)).

strength lies in its dynamic analysis, which explores the model's states and their stability in relation to changes in model parameters (Kerr et al., 2008, Nevado-Holgado et al., 2012, Abeysuriya et al., 2015).

In general, NFT can accommodate any number of neural populations and their connections. These can be used to represent cortical long-range (pyramidal) and short-range (interneuron) populations that may vary by cortical layer, structures such as the thalamus (including nuclei with different properties), the basal ganglia, and other subcortical structures. Additionally, NFT can model both uniform and nonuniform connectivities, providing flexibility in capturing complex neural interactions. Applications of these refinements and discussion of the issues involved can be found in previous studies (Deco et al., 2008, Albada and Robinson, 2009, Müller et al., 2017, Sanz-Leon et al., 2018, Robinson, 2019) and references cited therein. Notably, Sanz-Leon et al. (2018) provide insights into numerical implementations that are particularly useful for handling complex cases.

In the present work, we focus on EEG activity, which is known to be generated by large numbers of neurons in concert Nunez (1995) and is measured with centimeter-scale resolution. Hence, it is most appropriate to average over individual neural activities to obtain population-level signals that correspond to EEG, rather than modeling via individual spiking neurons (Nunez, 1995, Deco et al., 2008).

The CTM's ability to generate EEG-like signals has been demonstrated in numerous previous studies (Rennie et al., 2002, Robinson et al., 2002, 2004, Rowe et al., 2004, O'Connor and Robinson, 2005, Kerr et al., 2008). This model incorporates both long- and short-range cortical connections, as well as connections between the cortex and thalamic reticular and relay nuclei. At this level of refinement, we do not distinguish between various types of relay nuclei or account for spatial nonuniformities in connectivity parameters. Instead, we treat the model's physiological parameters as effective values that govern large-scale dynamics. These assumptions could be relaxed, but at a considerable cost in complexity, and the available data would not suffice to constrain the many additional parameters that would be needed.

The neural field $\phi(\mathbf{r}, t)$ $[\mathbf{s}^{-1}]$ represents a spatiotemporal neural activity propagating among neural populations when averaged across scales of approximately 0.1 mm. Within the framework of the CTM, four distinct neural populations are involved, with key connectivities, illustrated schematically in Fig. 2. These populations comprise excitatory (e) and inhibitory (i) cortical neurons, thalamic relay nuclei neurons (s), thalamic reticular nucleus neurons (r), and sensory inputs (n). Each of these populations has a soma potential $V_a(\mathbf{r}, t)$ $[\mathbf{V}]$ that is influenced by contributions ϕ_b from presynaptic populations, and generates outgoing neural activity $\phi_a(\mathbf{r}, t)$.

The dendritic spatiotemporal potential V_{ab} $[\mathbf{V}]$ is linked to the input ϕ_b through Equation 1. The parameter $\nu_{ab} = s_{ab}N_{ab}$ $[\mathbf{V}\cdot\mathbf{s}]$ represents the strength of the connection from populations b to a, where N_{ab} is the mean number of synapses per neuron a from neurons of type b, and s_{ab} $[\mathbf{V}\cdot\mathbf{s}]$ is the mean time-integrated strength of soma response per incoming spike. The parameter τ_{ab} $[\mathbf{s}]$ refers to the one-way corticothalamic time delay, and $D_a(t)$ is a differential operator, as described in Equation 2. Here, $1/\alpha$ and $1/\beta$ denote the characteristic decay time and rise time, respectively, of the soma response within the corticothalamic system.

Dendritic component:

$$D_a(t)V_{ab}(\mathbf{r}, t) = \nu_{ab}\phi_b(\mathbf{r}, t - \tau_{ab}) \tag{1}$$

$$D_a(t) = \frac{1}{\alpha\beta}\frac{d^2}{dt^2} + \left(\frac{1}{\alpha} + \frac{1}{\beta}\right)\frac{d}{dt} + 1 \tag{2}$$

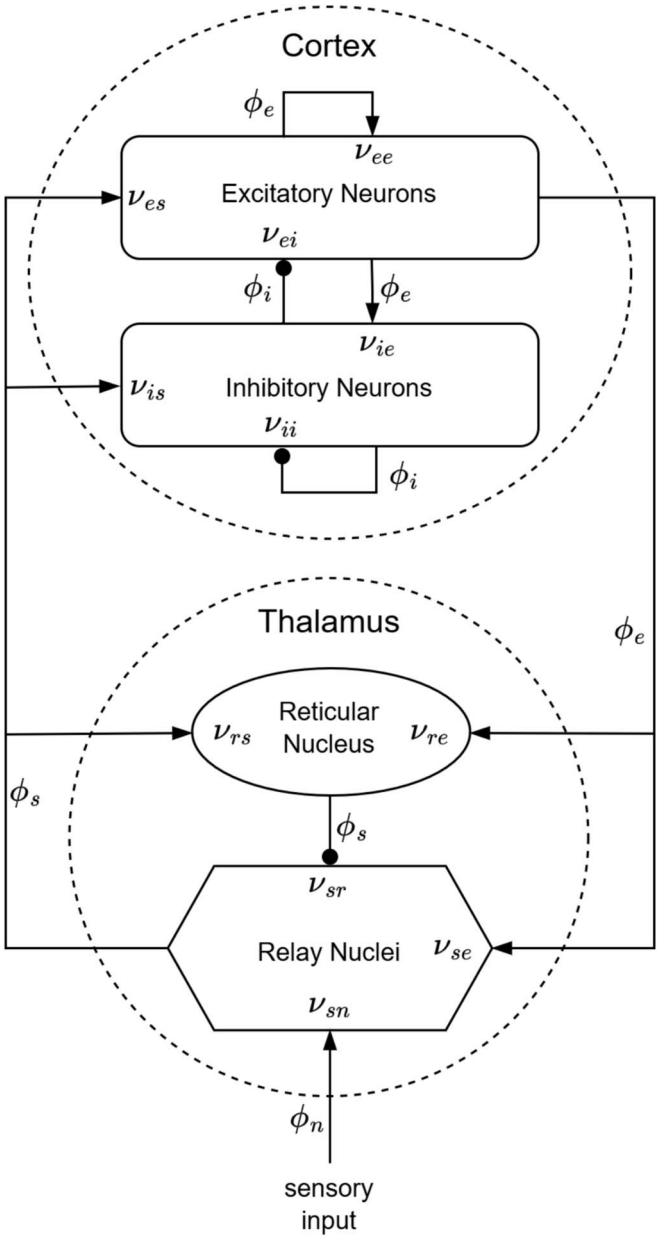

Figure 2. The CTM diagram. The neural populations shown are cortical excitatory, *e*, and inhibitory, *i*, thalamic reticular nucleus, *r*, and thalamic relay nuclei, *s*. The parameter ν_{ab} quantifies the strength of the connection from population *b* to population *a*. Excitatory connections are indicated by pointed arrowheads, while inhibitory connections are denoted by round arrowheads.

The soma potential V_a is determined as the sum of its dendrite potentials, as outlined in Equation 3. This potential undergoes some smoothing effects attributed to synaptodendritic dynamics and soma capacitance. Furthermore, the population generates spikes at a mean firing rate Q_a [$\mathbf{s}^{-1}$], which is related to the soma potential through a sigmoid function $S(V_a)$ (relative to the resting state), as shown in Equation 4. In this equation, $Q_{\max}$ denotes the maximum firing rate, while θ and $\sigma' \cdot \pi/\sqrt{3}$ correspond to the mean and the SD, respectively, of the firing threshold voltage.

Soma component:

$$V_a(\mathbf{r}, t) = \sum_b V_{ab}(\mathbf{r}, t) \tag{3}$$

$$Q_a = S(V_a) = \frac{Q_{\max}}{1 + e^{-(V_a - \theta)/\sigma'}} \tag{4}$$

The field ϕ_a approximately follows a damped wave equation with a source term Q_a, as detailed in Equation 5. The differential operator $D_a(\mathbf{r}, t)$ is defined in Equation 6, where v_a [$\mathbf{m} \cdot \mathbf{s}^{-1}$] represents the propagation velocity, r_a [$\mathbf{m}$] denotes the mean range, and $\gamma_a = v_a/r_a$ [$\mathbf{s}^{-1}$] signifies the damping rate.

Axonal component:

$$D_a(\mathbf{r}, t)\phi_a(\mathbf{r}, t) = Q_a(\mathbf{r}, t) \tag{5}$$

$$D_a(\mathbf{r}, t) = \frac{1}{\gamma_a^2}\frac{\partial^2}{\partial t^2} + \frac{2}{\gamma_a}\frac{\partial}{\partial t} + 1 - r_a^2\nabla^2 \tag{6}$$

In this model, only r_e is large enough to induce notable propagation effects. Consequently, the fields of other populations can be approximated as $\phi_a(\mathbf{r}, t) = S[V_a(\mathbf{r}, t)]$. Additionally, we assume

that the only non-zero time delays between populations are τ_{es}, τ_{is}, τ_{se}, and $\tau_{re} = t_0/2$, where t_0 is the total time it takes to traverse the corticothalamic loop. It is important to note that Equation 5 encompasses the intracortical time delays, as the wave equation inherently accounts for delays arising from propagation across the cortex. To further simplify the model, we assume random intracortical connectivity, leading to $N_{ib} = N_{eb}$ for all b (Braitenberg and Schüz, 1998). This assumption implies that the connection strengths are also symmetric, resulting in $\nu_{ee} = \nu_{ie}$, $\nu_{ei} = \nu_{ii}$, and $\nu_{es} = \nu_{is}$ (Robinson et al., 2005, Abeysuriya et al., 2015). Numerical integration (Sanz-Leon et al., 2018) or, when feasible, analytical integration (Robinson et al., 1997) of NFT equations produces a spatiotemporal activity signal that propagates across the cortical surface.

CTM EEG power spectrum

In scenarios of spatially uniform steady-state activity, it is possible to analytically compute the power spectrum of the model, eliminating the necessity for numerical integration. The steady state is attained by setting all time and space derivatives to zero. Employing the first term of the Taylor expansion enables a linear approximation of all potential perturbations from the steady state. Applying a Fourier transform to the model equations under these conditions yields Equation 7 for the dendritic component and Equation 8 for the axonal component. Within these equations, $\omega = 2\pi f$ denotes the angular frequency, $k = 2\pi/\lambda$ signifies the wave vector (λ is the wavelength), and $V_a^{(0)}$ represents the steady-state potential (Abeysuriya et al., 2015).

Dendritic equations in the frequency domain:

$$V_{ab}(\mathbf{k},\omega) = \nu_{ab}\phi_b(\mathbf{k},\omega)L(\omega)e^{i\omega\tau_{ab}} \tag{7}$$
$$L(\omega) = \left(1-\frac{i\omega}{\alpha}\right)^{-1}\left(1-\frac{i\omega}{\beta}\right)^{-1}$$

Axonal equations in the frequency domain:

$$D_a(\mathbf{k},\omega)\cdot\phi_a(\mathbf{k},\omega) = \rho_a V_a(\mathbf{k},\omega) \tag{8}$$
$$D_a(\mathbf{k},\omega) = k^2 r_a^2 + \left(1-\frac{i\omega}{\gamma_a}\right)^2$$
$$\rho_a = \frac{dS(V_a^{(0)})}{dV_a}$$

Using Equation 3, we can write Equation 8 as:

$$D_a(\mathbf{k},\omega)\cdot\phi_a(\mathbf{k},\omega) = \rho_a\sum_b V_{ab}(\mathbf{k},\omega) = \sum_b J_{ab}\phi_b(\mathbf{k},\omega) \tag{9}$$
$$J_{ab} = \rho_a\nu_{ab}L(\omega)e^{i\omega\tau_{ab}} = G_{ab}L(\omega)e^{i\omega\tau_{ab}}$$

Then, we can represent the interactions among the different populations within the CTM in matrix form:

$$\begin{bmatrix} D_e & 0 & 0 & 0\\ 0 & D_i & 0 & 0\\ 0 & 0 & D_r & 0\\ 0 & 0 & 0 & D_s \end{bmatrix}\cdot\begin{bmatrix}\phi_e\\ \phi_i\\ \phi_r\\ \phi_s\end{bmatrix} = \begin{bmatrix} J_{ee} & J_{ei} & 0 & J_{es}\\ J_{ie} & J_{ii} & 0 & J_{is}\\ J_{re} & 0 & 0 & J_{rs}\\ J_{se} & 0 & J_{sr} & 0\end{bmatrix}\cdot\begin{bmatrix}\phi_e\\ \phi_i\\ \phi_r\\ \phi_s\end{bmatrix} + \begin{bmatrix}0\\0\\0\\J_{sn}\phi_n\end{bmatrix} \tag{10}$$

Equation 10 can also be written in a compact form, when $\mathbf{J}^\star\boldsymbol{\phi}^\star$ is the external input to the CTM:

$$\mathbf{D}\boldsymbol{\phi} = \mathbf{J}\boldsymbol{\phi} + \mathbf{J}^\star\boldsymbol{\phi}^\star \tag{11}$$

By solving Equation 10, considering all the previously mentioned assumptions regarding D_a, ν_{ab}, and τ_{ab}, we can derive Equation 12. In this context, the quantities $G_{ese} = G_{es}G_{se}$, $G_{esre} = G_{es}G_{sr}G_{re}$, and $G_{srs} = G_{sr}G_{rs}$ correspond to the overall gains for the excitatory corticothalamic, inhibitory corticothalamic, and intrathalamic loops, respectively. The firing rate of sensory inputs to the thalamus, ϕ_n, is approximated by white noise. Without loss of generality, $\phi_n(\omega)$ can be set to 1, while only G_{sn} is subject to variation.

$$\phi_e(\mathbf{k},\omega) = \frac{G_{es}G_{sn}L^2e^{\frac{i\omega t_0}{2}}}{(1-G_{srs}L^2)(1-G_{ei}L)(k^2r_e^2+q^2r_e^2)}\phi_n(\mathbf{k},\omega) \equiv \Psi(\mathbf{k},\omega)\phi_n(\mathbf{k},\omega)$$
$$q^2r_e^2 = \left(1-\frac{i\omega}{\gamma_e}\right)^2 - \frac{1}{1-G_{ei}L}\left\{LG_{ee} + \frac{[L^2G_{ese}+L^3G_{esre}]e^{i\omega t_0}}{1-L^2G_{srs}}\right\} \tag{12}$$

The excitatory field ϕ_e is considered a good approximation of scalp EEG signals (Abeysuriya et al., 2015). The EEG power spectrum $P(\omega)$ (Equation 13) is calculated by integration of $|\phi_e(\mathbf{k},\omega)|^2$ over $\mathbf{k}$ when the cortex is approximated as a rectangular sheet of size $L_x \times L_y$. When considering periodic boundary conditions, this integral transitions into a summation over spatial modes with a discrete k. The filter function $F(k)$ serves as an approximation of the low-pass spatial filtering that occurs due to volume conduction through the cerebrospinal fluid, skull, and scalp.

$$P(\omega) = \sum_{m=-\infty}^{\infty}\sum_{n=-\infty}^{\infty}|\phi_e(k_x,k_y,\omega)|^2F(k)\Delta k_x\Delta k_y \tag{13}$$
$$k_x = \frac{2\pi m}{L_x},\ k_y = \frac{2\pi n}{L_y},\ k = \sqrt{k_x^2+k_y^2}$$
$$F(k) = e^{-k^2/k_0^2}$$

CTM stability

Prior research has demonstrated that the CTM can effectively describe both healthy and pathological brain activity. Healthy brain activity, such as wake–sleep cycles, corresponds to stable modes of the model, while pathological conditions, like epileptic seizures, are associated with unstable modes (Robinson et al., 2002, Breakspear et al., 2006).

The stability of the CTM is determined by the denominator in Equation 12. When all its zeros (Equation 14) satisfy $Im(\omega_0) < 0$, the model is stable:

$$(1-G_{srs}L^2)(1-G_{ei}L)(k^2r_e^2+q^2r_e^2) = 0 \tag{14}$$

Model stability boundaries can be represented approximately in a 3D space, as defined in Equation 15.

$$X = \frac{G_{ee}}{1-G_{ei}},\quad Y = G_{es}\frac{G_{se}+G_{sr}G_{re}}{(1-G_{srs})(1-G_{ei})},\quad Z = -G_{srs}\frac{\alpha\beta}{(\alpha+\beta)^2} \tag{15}$$

At $\omega = 0$, $L = 1$, so q^2 in Equation 12 can be written exactly in terms of the parameters X, Y, and Z. These parameters correspond to the strengths of the intracortical, corticothalamic,

and intrathalamic feedback loops, respectively. More generally, at low ω, they offer a qualitative representation of the majority of CTM's dynamics, provide insights into its stability characteristics across various parameter values, and determine key features of the power spectrum, such as resonance strength and damping. Furthermore, these reduced parameters allow for simplified interpretations of different brain states, including wakefulness, sleep stages, anesthesia, and DoC (Robinson et al., 2002, Abeysuriya et al., 2015, Abeysuriya and Robinson, 2016, Assadzadeh et al., 2023). We stress that the form of Equations 12 and 13 imply that the spectrum is a nonlinear function of X, Y, and Z.

A notable stability boundary in the CTM is represented by the equation $X + Y = 1$. At this boundary, a saddle-node bifurcation occurs, and the model exhibits the generation of epileptic seizures (Robinson et al., 2002). Interestingly, prior research has also demonstrated that both $X+Y$ and $X-Y$ can be utilized to distinguish between different states of consciousness (Assadzadeh et al., 2023).

Experimental data

In our study, we utilized a dataset consisting of open-eyes resting state high-density EEG recordings acquired from a total of 117 DoC patients and 23 healthy control subjects. The etiology of DoC patients included traumatic brain injury (TBI), stroke, anoxia, cardiac arrest, and other causes. The state of consciousness was assessed by experienced and trained clinicians using the Coma Recovery Scale-Revised (CRS-R) (Giacino et al., 2004) several times within a few days, including just before the EEG acquisition. All patients were medically stable, breathing spontaneously, and resided in hospitals, rehabilitation centers, or at home. The DoC patient group comprised 28 UWS patients (12 females, ages 21–73, CRS-R 4–9, 6 had TBI, 1–94 months since injury), 20 MCS– patients (11 females, ages 19–73, CRS-R 7–13, 9 had TBI, 1–103 months since injury), 50 MCS+ patients (19 females, ages 11–72, CRS-R 8–20, 23 had TBI, 1–156 months since injury), and 19 patients in eMCS (9 females, ages 12–66, CRS-R 16–23, 10 had TBI, 1–86 months since injury). The healthy control group consisted of 11 females and 12 males, aged between 19 and 69 years. Each participant's EEG activity was recorded using a Hydro-Cel GSN high-density electrode net (Electric Geodesics, EGI) equipped with 256 electrodes, with a sampling rate of 250 Hz. Data collection took place in a controlled environment, characterized by darkness and minimal sensory stimuli, with recording sessions lasting approximately 30 min. This dataset has already been utilized in several previously published studies (Carrière et al., 2020, Thibaut et al., 2021, Annen et al., 2023, Assadzadeh et al., 2023).

EEG processing

Each subject's EEG data went through several processing steps. First, we kept only 137 central electrodes and removed the rest in order to focus only on scalp-based electrodes. The signals from these electrodes were high-pass filtered above 0.2 Hz and notched at 50 Hz to eliminate line noise. Subsequently, to streamline computational processes, they were down-sampled to 125 Hz. The 30-min recording was then partitioned into nearly stationary sections (required for CTM fitting, which is performed through the steady-state activity power spectrum), with durations varying from 2.5 to 10 min. Detecting potential onsets of stationary sections involved splitting the electrode signals into 10-s segments and identifying when the segment's SD deviated by two SDs compared to the preceding segment. Defining stationary section boundaries required simultaneous onsets in more than 5% of the electrodes, with at least 2.5 min between onsets. Sections lasting between 10 and 20 min were equally divided into two, while those between 20 and 30 min were split into three sections.

The cleaning process for each stationary section of the data involved several sequential steps. Initially, noisy channels (electrode signals) were identified by segmenting the data into 5-s segments and calculating the SD of each channel within a segment. A channel within a segment was flagged as noisy if its SD exceeded seven times the SD of the entire non-segmented channel, or if it was three times higher than that of the other channels within the same segment. Segments with at least one noisy channel were deemed noisy, and entire channels were marked as noisy if more than 33% of their segments exhibited noise. These identified entire noisy channels were then removed and replaced with channels generated through a spherical spatial interpolation of the remaining channels. Subsequently, the data was re-referenced to the average of all channels and any remaining artifacts were eliminated. Artifacts were defined as 1-s segments where any sample's SD was five times greater than the channel's entire SD. To further refine the data, we conducted an independent component analysis to isolate and remove components associated with eye movements and non-EEG activity. After decomposition, we employed the *IClabel* toolbox (Pion-Tonachini et al., 2019) to retain only those components identified with at least 50% confidence as originating from genuine neural activity. The steps involving spatial interpolation, average referencing, and independent component analysis were all executed using the *EEGLAB* toolbox (Delorme and Makeig, 2004).

From the various stationary sections of each subject, we retained sections where fewer than 10% of the channels were flagged as noisy and fewer than 10% of the independent components were removed during the cleaning process. Among these sections, we selected the one with the least amount of detected artifacts per minute of recording. Then, we calculated the power spectra of all EEG channels in this selected stationary section using a fast Fourier transform, to be further used for CTM fitting.

Model fitting and signal generation

The CTM-fitting procedure was conducted by adjusting the analytical form of the CTM power spectrum (Equation 13) to match the power spectra of the stationary section within a frequency range of 1–40Hz. This fitting process was carried out using a Monte-Carlo Markov-Chain optimization procedure applied to model parameters, a method implemented in the *braintrak* toolbox (Abeysuriya and Robinson, 2016). We optimized the following model parameters: G_{ee}, G_{ei}, G_{es}, G_{se}, G_{sr}, G_{sn}, G_{re}, G_{rs}, α, β, t_0, and EMG_a. To support multi-electrode fitting, we assumed that G_{ee}, G_{ei}, G_{sn}, α, β, and t_0 exhibit a cosine-like variation over the scalp (O'Connor and Robinson, 2004).

Time series data were generated from the fitted model by numerically integrating its partial differential equations over time, incorporating the *NFTsim* toolbox (Sanz-Leon et al., 2018). The resulting artificial EEG signals, with a duration of 2.5 min, were sampled at 125 Hz and appeared at 784 locations on a 0.5 × 0.5 m square sheet. These signals were then interpolated to match the 137 experimental electrode locations, high-pass filtered above 0.2 Hz, and notched at 50 Hz, as we did in experimental data processing.

An illustrative example showing an experimental EEG Cz electrode power spectrum, a power spectrum derived from the fitted model, and a simulated EEG Cz electrode power spectrum is depicted in Fig. 3. The Cz electrode was specifically chosen to

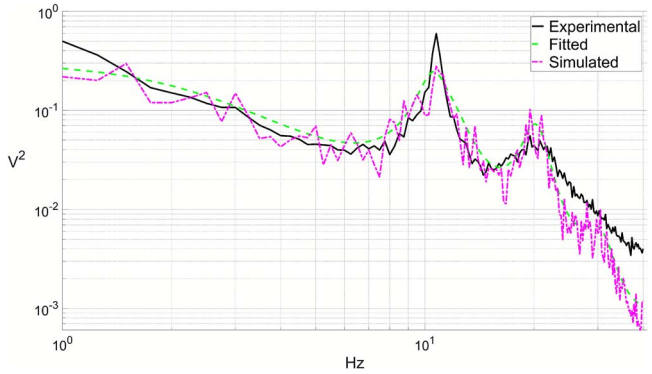

Figure 3. Experimental, fitted, and simulated power spectra. Example of a Cz electrode EEG power spectrum of a healthy wakeful subject, a fitted CTM power spectrum, and a Cz electrode power spectrum of a simulated EEG.

illustrate spectra of simulated data throughout this work, as its activity effectively represents the overall EEG activity generated by the CTM.

Feature extraction

Feature extraction plays a crucial role in our study, serving multiple purposes. First, these features are employed to gauge the state of consciousness in the subjects and their corresponding (fitted) CTMs. Next, we investigate correlations between features extracted from the experimental EEG and those derived from simulated EEG to evaluate how well a fitted CTM reproduces them. Lastly, we explore the impact of NFT parameters on various features by analyzing their interrelations. For each subject, the following features were extracted from both the experimental and the simulated EEG:

Spectrum-related features

For each EEG channel, we computed a normalized power spectrum and calculated the total power within the typical EEG bands: Delta (1–4 Hz), Theta (4–8 Hz), Alpha (8–12 Hz), Beta (12–24 Hz), and Gamma (24–40 Hz). Additionally, we calculated the spectral slope (the spectral exponent β) within the frequency range of 1–8 Hz using the FOOOF toolbox (Donoghue et al., 2020). Furthermore, we computed the spectral entropy of each EEG channel using the algorithm introduced by Piarulli et al. (2016). Despite being an entropy-related feature, we mention it here as it is derived from the power spectrum.

Entropy-related features

We calculated the permutation entropy (PE) from the time series of each EEG channel using Ouyang's toolbox (Ouyang et al., 2013). Additionally, we extracted Lempel-Ziv complexity (LZc) from all channels collectively using Fekete's toolbox (Fekete et al., 2018).

While all spectrum-related features and PE were computed for each EEG electrode, we opted to showcase the results specifically for the Cz electrode throughout this study. The Cz electrode effectively captures the overall EEG activity simulated by the CTM. On the other hand, experimental EEG activity may vary across the scalp; however, this variability is captured by multi-electrode fitting. Therefore, we allow ourselves to use this electrode to present experiment-based features as well, sacrificing some accuracy but gaining consistency with simulation-based features.

Parameter-feature correlation and sensitivity analysis

In order to understand how each NFT parameter influences the features extracted from simulated EEG, we performed a correlation analysis. This analysis involved calculating the Pearson correlation between different parameters and features, using data from all 140 subjects. However, it was necessary to ensure that the computed correlations were not a result of combinations of other NFT parameters. To address this, we also performed a comprehensive grid search across the parameter space and examined the sensitivity of features to various parameter values. To this end, we selected two representative subjects, one healthy and one MCS–, whose power spectra closely resembled the median power spectra of all subjects in the same state. We then utilized their fitted CTM to generate EEG signals and extract features while systematically altering the parameters one at a time. Each parameter was sampled from the entire possible parameter range while keeping the other parameters at their original fitted values. The altered parameters and their respective ranges are detailed in Table 1.

We computed parameter-feature correlations based on the sensitivity analysis of the two representative subjects and then compared them to ones acquired during an all-subjects correlation analysis. The goal was to identify whether there were similar or opposite trends in each parameter-feature correlation. With that said, it is important to note that the examination of only two subjects is not sufficient. To ensure the robustness of parameter-feature correlations, this procedure should ideally be conducted across the entire dataset. In this study, we illustrate the feasibility of trends comparison based on a sensitivity analysis using these representative subjects, recognizing that a comprehensive inspection of trends for every subject in the dataset is a substantial undertaking that exceeds the scope of our current work.

Results

We utilized NFT to model healthy wakefulness and consciousness-related brain injury states. By fitting a CTM to EEG data from 23 healthy subjects and 117 DoC patients, we investigated the correlations between fitted NFT parameters and features extracted from experimental and simulated EEG. Our analysis revealed significant correlations between various features and NFT parameters, particularly noting strong associations with stability-related parameters (X, Y, etc.), shedding light on the physiological basis of NFT parameters. By matching healthy and DoC states to these correlations, we have demonstrated the capabilities of NFT in representing healthy and impaired consciousness.

Discrimination of consciousness states

The initial investigation focused on determining whether any of the features or parameter ranges could effectively differentiate between different DoC (UWS, MCS–, MCS+, eMCS) and healthy wakefulness states. We assessed whether features derived from experimental EEG signals, fitted NFT parameters, and features obtained from simulated EEG signals could act as reliable biomarkers for states of consciousness. Through statistical analysis using a non-parametric permutation test (10^4 permutations) with false discovery rate multiple comparisons correction (Groppe et al., 2011), many of these features and parameters demonstrated the capacity to differentiate between DoC and healthy wakeful individuals with statistical significance. However, none of the

Table 1. Altered parameters and their ranges.

Parameter	Description	Range
$G_{ee} = \rho_e \nu_{ee}$[a]	Excitatory cortical gain	0–20
$G_{ei} = \rho_e \nu_{ei}$	Inhibitory cortical gain	(–20)–0
$G_{es} = \rho_e \nu_{es}$	Thalamic relay nuclei to cortex connection gain	0–11
$G_{se} = \rho_s \nu_{se}$	Cortex to thalamic relay nuclei connection gain	0–17
$G_{sr} = \rho_s \nu_{sr}$	Reticular to relay intrathalamic nuclei connection gain	(–9)–0
$G_{re} = \rho_r \nu_{re}$	Cortex to thalamic reticular nuclei connection gain	0–7
$G_{rs} = \rho_r \nu_{rs}$	Relay to reticular intrathalamic nuclei connection gain	0–8
α	Inverse synaptodendritic decay time	10–120
β	Inverse synaptodendritic rise time	100–800
t_0	Corticothalamic loop delay	0.075–0.14

[a] ν_{ab} denote the connection strengths between the different CTM populations (see Fig. 2), and ρ_a is defined in Equation 8.

features or parameters were successful in differentiating between individual DoC states.

Features from experimental and simulated EEG

Figure 4a and b presents features that exhibited significant differences between DoC and healthy wakefulness states when extracted from both experimental and simulated EEG. The spectrum-related features delta-power, alpha-power, beta-power, spectral slope, and spectral entropy prove effective discrimination in both the experimental and the simulated cases. This alignment was expected due to the CTM fitting process, which utilizes the spectrum. The entropy-related features also exhibit discriminative abilities between DoC and healthy states. Intriguingly, the discriminative power of the PE feature is statistically significant solely when calculated from experimental EEG data, whereas the LZc feature exhibits significance solely when computed from simulated EEG data.

NFT parameters

During this study, we observed that the repeated fitting of the CTM to experimental EEG data did not converge to a single set of parameters, in alignment with previous findings (Abeysuriya et al., 2015, Abeysuriya and Robinson, 2016). Instead, it produced a broad range of parameter values with a complex distribution, while the goodness of fit (χ^2) remained relatively stable (see Fig. 5). Hence, distinguishing between states of consciousness using NFT parameters could only be possible by using a sophisticated classifier. However, this approach is outside of the scope of the current work.

Nonetheless, we aimed to identify typical parameter value ranges for different states of consciousness. To achieve this, we repeated the fitting process 15 times for all subjects. Figure 6 illustrates NFT parameters with significantly distinct ranges for DoC and healthy wakefulness states. (During the statistical analysis, we permuted all the 15 fits of a subject together.) Similar to the extracted features, the fitted NFT parameters could discriminate only between healthy and DoC states, but not among different DoC substates.

Feature reproduction from simulated EEG

We explored correlations between features extracted from experimental EEG data and simulated EEG data. Notably, most of the spectrum-related features showed significant correlations. Specifically, Delta-power, Theta-power, Alpha-power, Beta-power, spectral slope, and spectral entropy features exhibited correlations with $R > 0.71$ ($p < 10^{-23}$), and their simulation-based values closely resembled the experiment-based results. In contrast, the Gamma-power feature did not display any significant correlations.

Among the entropy-related features, only LZc presented a substantial correlation of $R = 0.63$ ($p < 10^{-16}$), as depicted in Fig. 7. While its simulation-based values were biased and exhibited shrinkage relative to the experiment-based ones (i.e. the linear fit curve did not align with the $x = y$ line), a simple linear transformation could rectify this misalignment.

Parameter-feature correlations analysis

We discovered significant correlations ($p<.001$) between fitted parameters and features extracted from EEG generated by a fitted CTM. The Pearson correlation coefficients R for these relationships are provided in Table 2. Notably, NFT parameters that presented many correlations with the features tend to be stability-related (X, Y, Z, etc.).

The majority of these correlations were validated through sensitivity analysis. Both of the representative subjects showed similar trends, with correlation coefficients maintaining the same sign and high statistical significance ($p<.05$). Some of the correlations were not confirmed (indicated by ♣ in Table 2), but they were not contradicted either. In these cases, correlations were either insignificant or did not exhibit a clear monotonic trend, but neither did the healthy subject nor the MCS– patient display monotonic trends with opposite signs to the ones observed in the all-subjects correlation analysis. For instance, no significant correlation was observed between the excitatory cortical gain G_{ee} and the Theta-power feature during the sensitivity analysis of a healthy subject. Interestingly, the trends comparison based on the sensitivity analysis revealed strong correlations that were not evident in the initial analysis with all subjects, such as those between G_{ee} and Beta-power (see Fig. 8). The reasons for these discrepancies are explored in the Discussion section.

Table 2 also includes the expected correlation trends of NFT parameters. In the section related to differentiating consciousness states, we showed that G_{es}, G_{ese}, G_{rs}, Y, and Z are positively correlated with the level of consciousness, whereas G_{ee}, G_{esre}, G_{srs}, t_0, X, and $X-Y$ are negatively correlated with it.

Furthermore, in the table, we included the expected correlations of various features with the levels of consciousness, as reported in the existing literature. Previous research has indicated a positive correlation between the level of consciousness and the features: Alpha-power, Gamma-power (Bai et al., 2021), spectral slope (Gao et al., 2017, Colombo et al., 2019), spectral entropy (Piarulli et al., 2016, Martens et al., 2021), PE, and LZc (Mateos et al., 2018). Conversely, a negative correlation has been observed between consciousness level and the features: Delta-power and

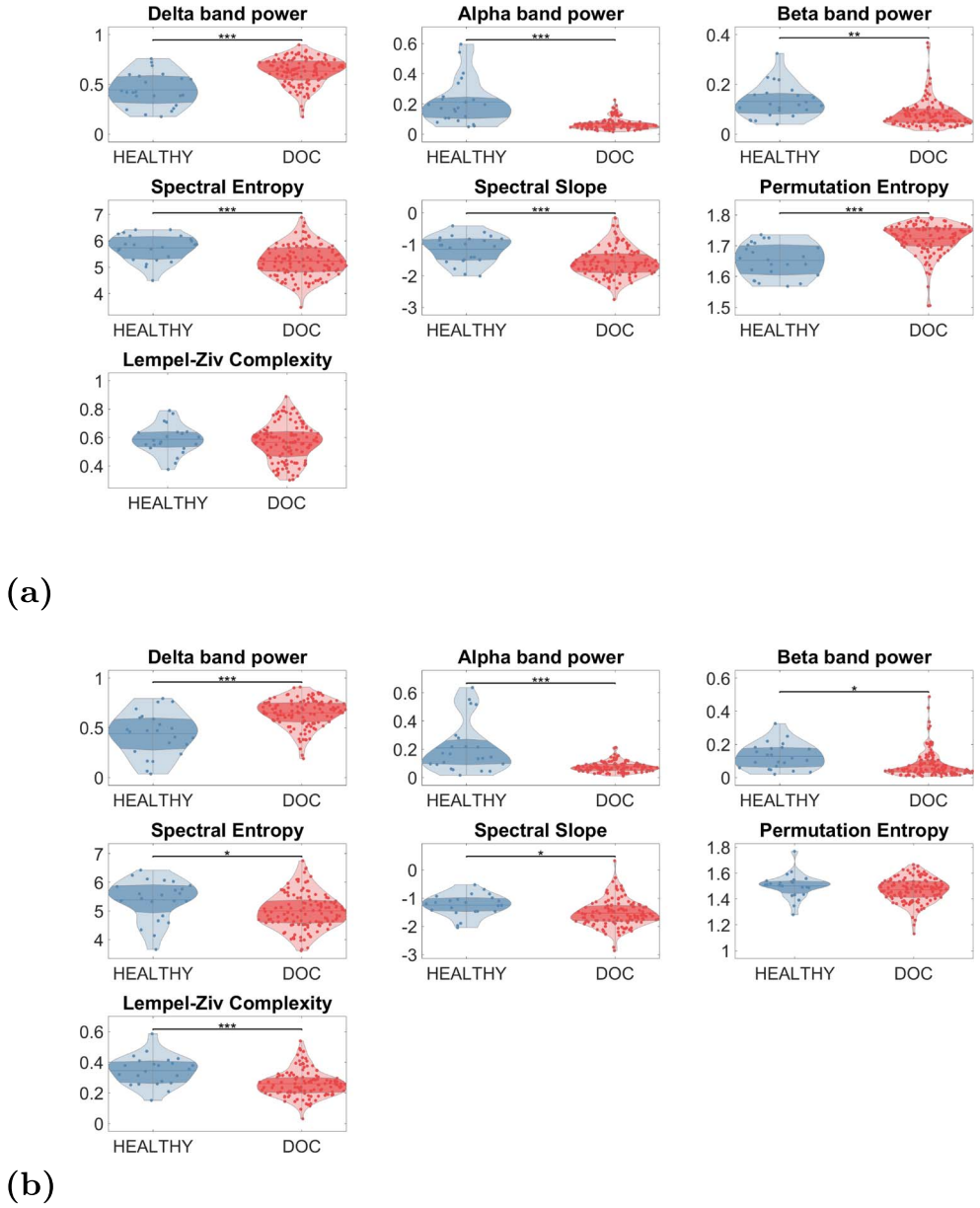

Figure 4. Differentiation of DoC states from a healthy wakefulness state. The compared features were extracted from (a) experimental EEG and (b) CTM-simulated EEG.

Theta-power (Bai et al., 2021). However, almost half of these features (marked with ♠) did not exhibit significant discrimination abilities between consciousness states, as demonstrated above. Furthermore, the experiment-based permutation entropy of DoC states was significantly higher than that of healthy wakefulness state, contradicting previous findings (Mateos et al., 2018). This discrepancy discredits the correlation between simulation-based PE and consciousness level.

All of the identified correlations align with the expected correlation trends stemming from theoretical foundations, prior studies, and the results of consciousness state discrimination. For instance, we observed a positive correlation between spectral entropy and Z, which matches the positive correlation between consciousness level and both of them. However, the spectral entropy correlation with X was negative, which corresponds to a positive correlation between consciousness level and spectral entropy on one hand, and a negative correlation between consciousness level and X on the other hand. In general, we expected that parameter-feature correlations would exhibit positivity when both consciousness-feature and consciousness-parameter correlations are either positive or negative, and exhibit negativity when one of these correlations is positive while the other is negative. It is noteworthy that correlations between consciousness and features that were not confirmed by consciousness states discrimination (marked with ♠) suggest that the dataset did not reflect the anticipated relations from existing literature and were thus not utilized to test for mismatching.

Discussion

In this work, we have delved into the application of NFT modeling in the study of the neural correlates of consciousness. Despite its inherent simplicity as a brain model, NFT has shown promising potential for representing consciousness states. The model's

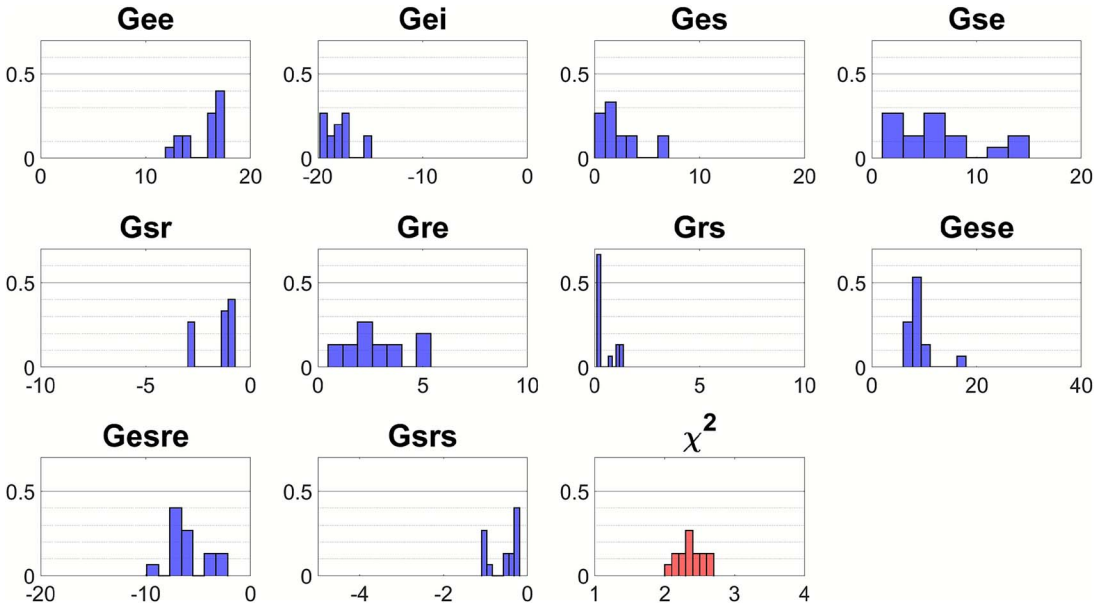

Figure 5. Distribution of NFT parameters obtained from 15 repeated fitting processes on a single MCS+ patient. Most parameters exhibited a wide distribution, covering a substantial portion of the typical range, and featuring several prominent peaks. The different gain terms G_{ab} are defined in Table 1, while composite gains are defined as $G_{ese} = G_{es}G_{se}$, $G_{esre} = G_{es}G_{sr}G_{re}$, and $G_{srs} = G_{sr}G_{rs}$.

ability to capture healthy and injured brain with impaired consciousness states was evident through fitted NFT parameters and features based on simulated EEG, which exhibited discrimination capabilities and significant correlations. The NFT parameters also offered physiological interpretations for features based on simulated EEG and the states of consciousness. These various feature and parameter correlations underscore the suitability of NFT for advancing research in the field of consciousness, serving both as a tool for hypothesis generation and for conducting *in-silico* experiments.

Feature-based discrimination of consciousness states

Many of our results align with previous findings. It was established in prior research that Alpha-power, spectral slope, and spectral entropy tend to have higher values in states of high consciousness and lower values in states of low consciousness, while the opposite is observed for Delta-power (Piarulli et al., 2016, Gao et al., 2017, Darracq et al., 2018, Colombo et al., 2019, Bai et al., 2021, Martens et al., 2021). In our study, we observed these behavior in both the features extracted from experimental EEG data and those derived from simulated EEG data. This alignment was expected, given that we employed the CTM's power spectrum for model fitting (see Fig. 3).

The LZc feature results were consistent with prior research, showing higher LZc values associated with higher consciousness levels and lower values with lower consciousness levels (Mateos et al., 2018). Interestingly, only the simulated-EEG-based LZc exhibited statistical significance ($p < .001$) in distinguishing between healthy and DoC states. However, we showed that experimental-EEG-based LZc has a correlation of $R = 0.63$ with simulated-EEG-based LZc. A potential explanation for this disagreement could be that experimental data may contain noise and biases that impact the LZc feature, which are filtered out during the fitting process. This implies that the fitted CTM might emphasize LZc as a potential biomarker for its inherent consciousness level.

Intriguingly, we observed a divergence from existing literature concerning the PE feature, with lower values observed in healthy subjects and higher values in DoC patients. This contradicts previous findings, which typically report the opposite trend (Mateos et al., 2018). Unfortunately, we were unable to provide a definitive explanation for this discrepancy. Further investigation is warranted to elucidate the underlying reasons for this unexpected finding.

It is important to note that the ability to distinguish between healthy and DoC states, while not being able to differentiate among DoC substates, aligns with expectations for these features. The classification of DoC substates based on EEG features remains a challenging task, with limited success achieved so far, typically in conjunction with a preceding transcranial magnetic stimulation (Casali et al., 2013). Therefore, the capability to differentiate between healthy wakefulness and DoC states based on resting-state EEG data, whether experimental or simulated, is consistent with most findings in this field.

Parameter-based discrimination of consciousness states

We successfully replicated the main findings of similar research previously conducted by Assadzadeh et al. (2023). In their study, Assadzadeh analyzed subjects from the same DoC database, fitted CTMs to these subjects, and applied a linear discrimination analysis on NFT parameters to classify various DoC and healthy wakefulness states. By combining $X - Y$, $X + Y$, and $1/\alpha + 1/\beta$, they achieved a classification accuracy of 93% for distinguishing between DoC and healthy states, but not among different DoC substates (Assadzadeh et al., 2023). While achieving high classification accuracy of consciousness states was not the primary focus, of the current study, a combination of various features and NFT parameters could potentially yield promising results in this regard.

Instead, our focus was on understanding how each of the NFT parameters reflects the state of consciousness, and our findings were consistent with those presented by Assadzadeh et al. (2023)

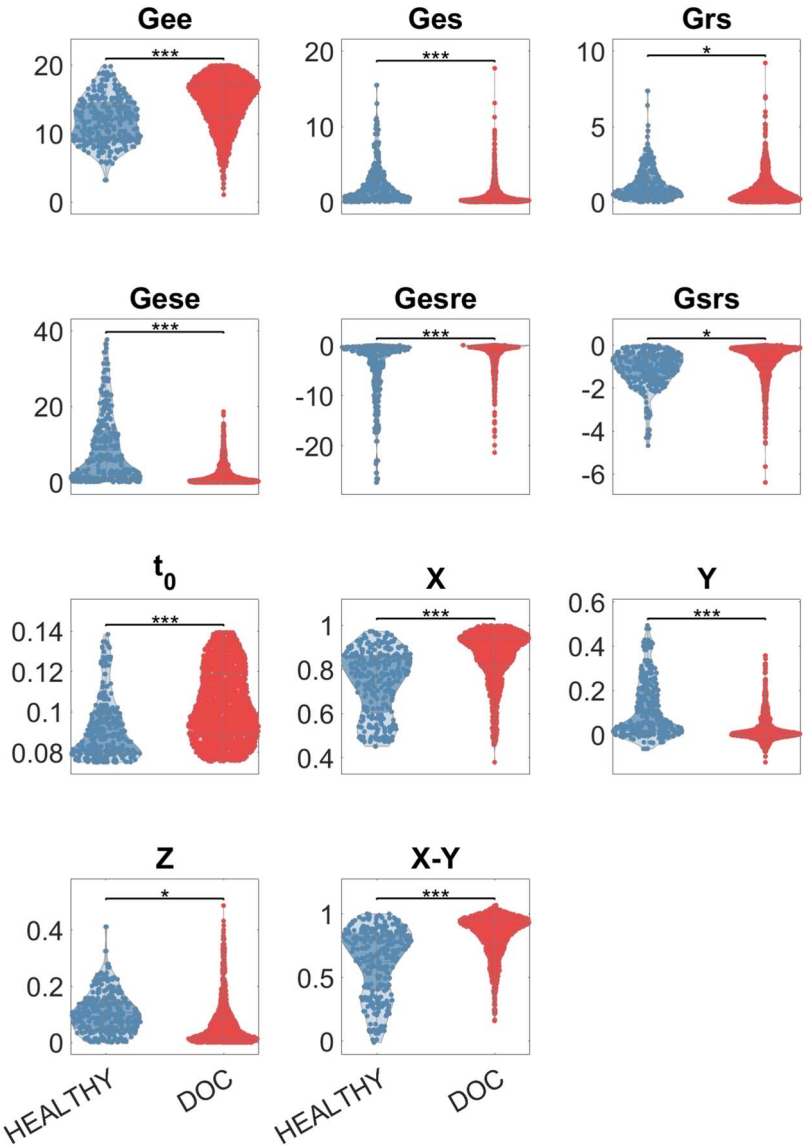

Figure 6. Differentiation of DoC states from a healthy wakefulness state based on fitted NFT parameters. For each subject, 15 different sets of parameters were obtained during repeated fitting processes. Discriminatory capabilities primarily rely on combinations of parameters, such as G_{esre} or X,Y, Z.

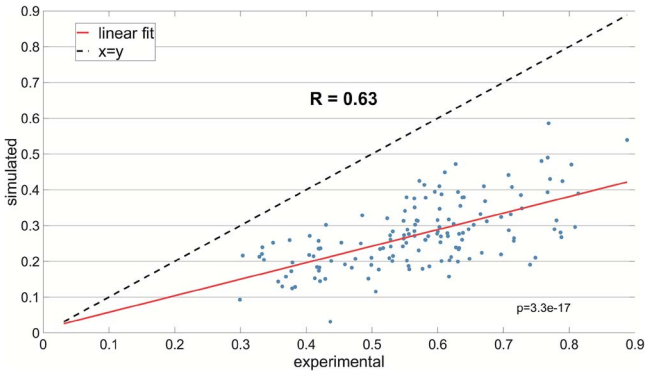

Figure 7. Correlation between LZc derived from experimental EEG data and LZc obtained from EEG data generated from a fitted CTM. The linear fit line illustrates the relationship between the two sets of data.

We discovered, akin to their results, that the gain parameters G_{ee}, G_{ese}, G_{esre}, G_{srs}, and the stability parameters X,Y, Z, and $X - Y$, all exhibited significantly divergent ranges of values ($p < .05$) between DoC and healthy states. Additionally, we identified significant discriminatory capabilities between healthy and DoC states through the G_{es}, G_{rs}, and t_0 parameters. This suggests that each of these parameters contributes to the representation of the state of consciousness within the CTM, offering valuable physiological insights.

These results can be explained physiologically within the framework of the CTM. The high intracortical feedback loop strength X observed in DoC patients suggests that the cortex becomes increasingly self-driven, exhibiting strong intracortical coupling while being disconnected from external inputs and feedback mechanisms (Robinson, 2017). This aligns with previous findings that one of X's components, the excitatory intracortical gain G_{ee}, is larger in deep sleep (Abeysuriya et al., 2015). Conversely, the high corticothalamic feedback loop strength Y in healthy wakeful subjects reflects positive feedback between the cortex and thalamus, which is crucial for maintaining the connection to the external world (Robinson et al., 2002). This is further supported by the fact that the corticothalamic loop gains G_{ese} and G_{es}, both of which are larger in healthy

Table 2. Parameter-feature correlations.

	Delta power	Theta power	Alpha power	Beta power	Gamma power	Spectral slope	Spectral entropy	Permutation entropy	Lempel-Ziv complexity	Consciousness vs parameter
G_{ee}	0.47	–0.44♣				–0.48			–0.34	negative
G_{ei}										
G_{es}										positive
G_{se}										
G_{ese}										positive
G_{sr}								–0.28		
G_{re}										
G_{esre}										negative
G_{rs}							0.27		0.3	positive
G_{srs}	0.63		–0.4♣	–0.76	–0.27	–0.3	–0.61	–0.5	–0.65	negative
α				0.3				0.8		
β								0.55		
t_0			–0.3							negative
X	0.61	–0.65	–0.5			–0.7	–0.25		–0.39	negative
Y	–0.6♣		0.55			0.6♣				positive
Z	–0.58			0.75	0.3		0.62	0.5	0.65	positive
X + Y	0.53	–0.59				–0.46			–0.34	
X – Y	0.66	–0.58	–0.56			–0.7			–0.36	negative
Consciousness vs feature	negative	negative♠	positive		positive♠	positive	positive	positive♠	positive	

The table illustrates correlations between NFT parameters and features extracted from simulated EEG obtained from CTMs fitted to different subjects. Correlations that were not confirmed through the sensitivity analysis are marked with ♣. All the presented correlations are statistically significant (p <.001). The "consciousness vs parameter" column denotes the correlation between consciousness level and various NFT parameters, as observed in the "Discrimination of consciousness states" section. The "consciousness vs feature" row represents the expected correlations between features and the level of consciousness, as outlined in the literature. Consciousness-feature correlations that were **not** observed during consciousness states discrimination are marked with ♠.

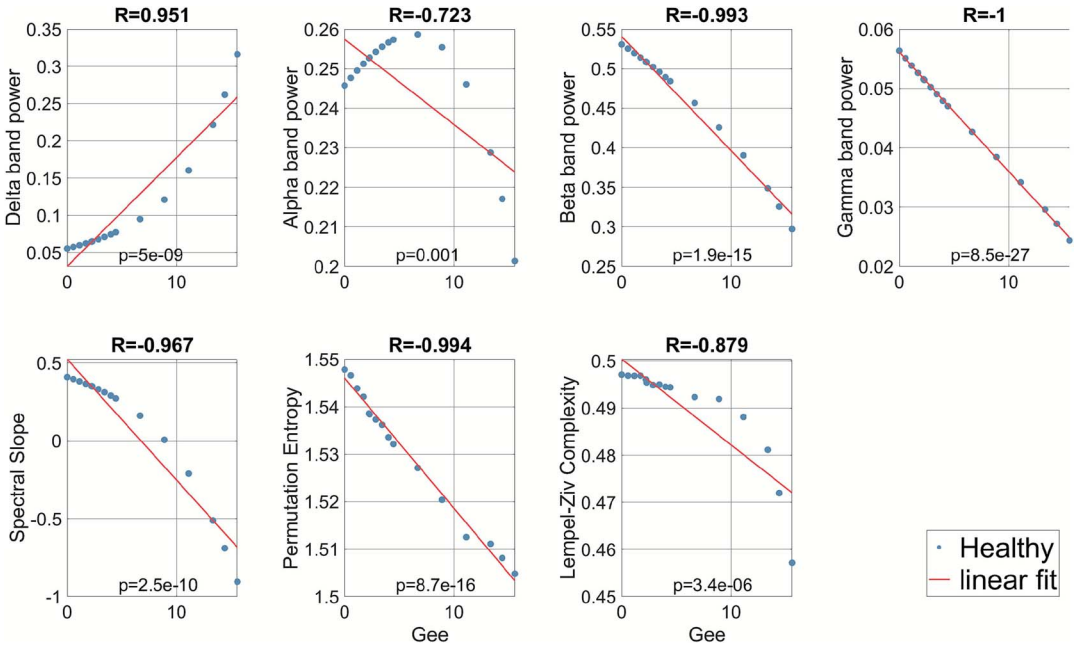

Figure 8. G_{ee} parameter sensitivity of features extracted from simulated EEG. The CTM was fitted to a healthy wakeful subject. Only correlations with p <.05 are presented.

individuals. Additionally, the increased negative corticothalamic feedback G_{esre} in healthy subjects suggests greater inhibition exerted by the thalamic reticular nucleus, a hallmark of wakeful vigilance (Assadzadeh et al., 2023, Whyte et al., 2024). Together, these observations explain why the difference $X - Y$ effectively parametrizes the level of consciousness, as the largest variance occurs along this axis (Assadzadeh et al., 2023). Interestingly, prior studies have shown that healthy wake-state brain activity lies close to the stability boundary $X + Y = 1$, corresponding to a near-critical state (marginal stability) (Gervais et al., 2023). Consequently, Y is anticorrelated with X to maintain the linear stability of the CTM (Breakspear et al., 2006, Shriki and Yellin, 2016, Robinson, 2017, 2021).

Regarding other parameters, the high intrathalamic feedback loop strength Z in healthy wakeful individuals is consistent with previous findings showing that Z is lower in deep sleep but higher during REM sleep and wakefulness. Similar trends have been observed in Z's components, including the intrathalamic loop gain G_{srs} and excitatory relay-to-reticular intrathalamic gain G_{rs} (Abeysuriya et al., 2015). Finally, the increased corticothalamic

loop delay (t_0) observed in DoC patients may be attributed to the additional latency from damaged corticothalamic connections, potentially contributing to reduced consciousness.

It is essential to bear in mind that while we identified typical parameter ranges for DoC and healthy subjects, we should not depend on a single parameter value for determining the state of consciousness. As demonstrated, CTM parameters can converge to different values for the same subject. We speculate that these different values, when combined with other parameters, form a manifold that represents a state of consciousness. It is possible that parameter combinations such as $X - Y$ partially describe this manifold, providing them with the capability to differentiate between states of consciousness.

Features reproduction

We aimed to investigate whether a CTM fitted to a particular subject can produce EEG features with values that closely match those obtained from experimental EEG. Our analysis identified strong correlations between all the spectrum-related features, except Gamma-power, extracted from both experimental EEG and simulated EEG data. Additionally, a notable correlation was observed between the LZc feature derived from both types of data. The strong correlation and the close match between the experiment-based and simulation-based spectrum-related feature values was anticipated, given that the CTM was fitted based on the power spectrum. The lack of correlation for Gamma-power might be explained by the fitting objective function, which assigns more weight to lower frequency power than to higher frequency power (Abeysuriya and Robinson, 2016). The impact of this weighting is evident in Fig. 3, where the frequencies in the Gamma band of the analytical and simulated spectra do not follow the experimental spectrum.

The correlation discovered for LZc is quite interesting and meaningful. It suggests that, in EEG-based research, simulated EEG can be used as a viable alternative to experimental EEG when employing LZc as a measure. Furthermore, if a CTM is utilized for *in-silico* experiments, LZc can act as a valuable biomarker for the level of consciousness, paralleling its extensive use in prior studies on the NCC (Casali et al., 2013, Schartner et al., 2017, Fekete et al., 2018, Li and Mashour, 2019, Medel et al., 2023). This finding also indicates that the fitted CTM has the capability to control the complexity of the generated signal using its parameters. We present these parameters in Table 2, offering a physiological interpretation for LZc.

Parameter-feature correlations

In this part, our aim was to investigate how each fitted parameter influences the features computed from simulated EEG. As mentioned earlier, most of the features exhibit correlations with NFT parameters, and these correlations offer valuable insights into the physiological explanations for each feature. For instance, we found that PE is moderately affected by G_{sr}, G_{srs}, *NFT* α, *NFT* β, and *NFT Z*, which represent the thalamic reticular-relay nuclei connection gain strength, intrathalamic loop gain strength, synaptodendritic decay and rise rates, and intrathalamic feedback loop strength, respectively. The positive correlations between PE and *NFT* α and β make intuitive sense: higher synaptodendritic response rates lead to faster alterations in the output signal, resulting in a more complex and informative signal, which translates to higher entropy. Additionally, the positive correlation between PE and *Z* (and its negative correlation with *Z*'s components G_{sr} and G_{srs}) can be explained by the role of *Z* in governing spindle instability (Robinson et al., 2002, Abeysuriya et al., 2015). An increase in spindle activity introduces greater variability into the signal, thereby elevating its entropy.

A notable point from Table 2 is the dominant role of stability-related parameters *X*, *Y*, *Z*, and their combinations in driving the majority of correlations observed. This aligns with prior research suggesting that *X*,*Y*, and *Z* qualitatively encapsulate a significant portion of CTM's dynamics and provide simplified representations of various states of consciousness (Robinson et al., 2002, Abeysuriya and Robinson, 2016, Assadzadeh et al., 2023). This observation supports our hypothesis that a single parameter may not fully represent a specific model behavior; instead, a set of parameters, potentially forming a complex manifold, might be required. However, this does not diminish the importance of correlations involving other individual parameters, which also play a critical role in elucidating various features, as previously discussed.

We compared our results to those from parameter sensitivity analyses in previous studies. Robinson et al. (2001) explored how different parameters affect the analytical power spectrum of a simplified CTM (excluding the thalamic reticular nucleus) fitted to a healthy, awake, eyes-closed subject. Subsequently, Rowe et al. (2004) performed a similar analysis on the complete CTM, replicating Robinson's findings and exploring additional parameters. Most of the correlations we identified between spectrum-related features and NFT parameters were consistent with these studies (except for spectral entropy, which was not analyzed by Robinson and Rowe). However, some correlations reported there are not evident in our results. These include correlations of G_{ee} with Alpha-power, t_0 with Delta and Theta-power, *NFT* α with Gamma-power, and all correlations involving G_{ei}, G_{ese}, G_{esre}, and *NFT* β. Additionally, we identified correlations (albeit low) of G_{srs} with Gamma-power and spectral slope that were not reported previously. These discrepancies might stem from the significantly different experimental conditions between our study and previous ones, as well as from our reliance on simulated data of multiple subjects versus the analytical spectrum of a single subject used in the earlier research.

In the sensitivity analysis, we explored the parameter space around a fitted parameter set. This parameter corresponds to a fixed point on a manifold, representing all possible parameter combinations that produce a fitted spectrum. Such fixed points on the manifold may exhibit varying degrees of sensitivity to individual parameters. By selecting a different point on the manifold, or simply by exploring the fitted parameters of another subject, we may encounter heightened sensitivity to certain parameters, while observing reduced sensitivity to others. The overall trend encompasses various fixed points for all of the different subjects, yet not all of these points demonstrate sensitivity to the same parameters.

This perspective can also offer an explanation for correlations that appeared during the sensitivity analysis, but were absent in Table 2. For example, the correlation between G_{ee} and Beta-power, as seen in Fig. 8, reflects the behavior of parameters around a fitted parameter set of a particular healthy subject. However, this behavior is not universal across all subjects, indicating that the correlation is subject-specific and not generalizable. Consequently, the examination of trends through the sensitivity analysis should ideally be extended to encompass all subjects within the dataset to validate the overall parameter-feature correlations, as previously emphasized.

The alignment of the discovered correlations with the anticipated trends from the NCC and the consciousness states' discrimination results underscores the NFT model's potency to

represent healthy wakefulness and brain injury with impaired consciousness. The triadic relationship observed between parameter values, consciousness levels, and feature values means that both a fitted NFT parameter and a simulated-EEG-based feature can effectively represent the consciousness state, with changes in one being reflected in the other.

Consciousness state representation in the NFT model

Our findings indicate that the CTM effectively captures both healthy and impaired states of consciousness. However, it falls short in distinguishing between specific DoC substates (UWS, MCS–, MCS+, eMCS), limiting its capacity to represent varying degrees of impaired consciousness beyond a general distinction between healthy and brain-damaged states. This limitation is evident in analyses using both NFT parameters and features derived from simulated EEG data. Enhancing the CTM by incorporating additional brain regions, increasing its spatial resolution, and explicitly modeling the affected and intact areas of the brain (O'Connor and Robinson, 2005, Albada and Robinson, 2009, Robinson et al., 2011) may improve its ability to represent different DoC and additional consciousness states.

A related consideration concerns the special case of eMCS. As noted in the Introduction, we include eMCS within the DoC spectrum for the purposes of this study, given that these patients have a history of consciousness impairment due to brain injury, even though they are clinically considered fully conscious (Giacino et al., 2004, Bodien et al., 2020). This choice is supported by our findings, which show that the features and NFT parameter values of eMCS patients more closely resemble those of other DoC patients than those of healthy controls. This suggests that, despite behavioral recovery, eMCS patients may retain neural activity patterns characteristic of brain injury. Further investigation is needed to determine whether the CTM is capturing residual effects of consciousness-related brain injury or potentially revealing novel neural aspects of the eMCS state.

Nonetheless, the CTM's ability to reflect both healthy and impaired consciousness states through features derived from simulated EEG remains highly valuable. Furthermore, we found that these features are influenced by NFT parameters, which exhibit distinct value ranges corresponding to different states of consciousness. This triadic relationship offers verification of the model's ability to faithfully reflect the state of consciousness of the subject to which it is fitted.

A particularly interesting example is the LZc feature, which effectively discriminates between DoC and healthy subjects. It correlates with G_{srs} and stability-related NFT parameters, all of which demonstrate the capability to distinguish between impaired and healthy consciousness states as well. Moreover, a robust correlation exists between simulated-EEG-based LZc and experimental-EEG-based LZc. Thus, LZc extracted from simulated data emerges as a reliable biomarker for assessing the consciousness state within the CTM, akin to its utility in previous NCC-related studies.

The compelling evidence presented in this study lends credibility to the use of NFT as a valuable tool in consciousness research for applications that include model-based interpretations, hypothesis generation, and *in-silico* experiments. For example, consider a scenario where researchers aim to investigate the effects of a drug that suppresses intrathalamic feedback mechanisms on the level of consciousness. A CTM could be fitted to a healthy subject, and G_{srs} could be manipulated to generate an EEG time series. Then, LZc for various G_{srs} values could be calculated, and the consciousness level could be determined accordingly. In another scenario, if a subject has been administered propofol and exhibits an observable increase in Delta-power, the fitted CTM may suggest that the subject's condition can be explained by high intracortical feedback loop strength X. However, Delta-power is also influenced by G_{srs}. Therefore, researchers may hypothesize that administering the studied drug to the propofol-anesthetized subject will reverse the observed effects and potentially wake her/him up.

Overall, the utilization of a reliable computational brain model in consciousness research offers numerous advantages, whether seeking model-based predictions or investigating the neural mechanisms underlying a phenomenon. When it comes to experiments involving live subjects, the model helps to avoid potential health risks and negative implications. Furthermore, for other experiment types and theoretical work, computational modeling can significantly save time, effort, and expenses. The prospects of integrating NFT modeling into consciousness research are promising. We anticipate that future research endeavors will increasingly harness NFT to gain deeper insights into the intricate nature of consciousness and contribute to advances in the field of the NCC. Yet, a more immediate research direction should include a similar exploration of data from other consciousness-related states, such as sleep, anesthesia, and psychedelics, to inspect how the CTM represents them and to enhance our understanding of the brain's functioning across these states of consciousness.

Conclusion

In this study, we explored the application of NFT modeling in investigating and understanding the NCC. Despite its inherent simplicity, NFT has shown considerable promise in representing consciousness states in the brain.

Our primary findings indicate that CTM is capable of reflecting healthy and impaired consciousness states, both in terms of fitted NFT parameters and features derived from simulated EEG. These features have exhibited discrimination capabilities and have shown significant correlations with model parameters, highlighting CTM's potential as a model for understanding and representing consciousness.

Our results suggest that NFT can be a valuable tool in consciousness research, supporting model-based interpretations, hypothesis generation, and *in-silico* experiments. This study establishes a strong foundation for further exploration of NFT, offering new insights into consciousness and the brain's dynamics. By deepening our understanding of these relationships, this research could inspire innovative approaches in neuroscience, cognitive science, and consciousness studies.

Acknowledgments

We would like to thank Dr. Eli J. Müller from the Brain and Mind Centre at the University of Sydney for providing invaluable insights into the NFT framework software. We also extend our gratitude to Dr. Jitka Annen and Dr. Glenn van der Lande for their efforts in data curation. Additionally, Dr. Annen provided valuable feedback throughout the research process and during the preparation of this manuscript. O.G. is a research associate and S.L. is a research director at FRS-FNRS. The wording revision process of this article included the use of ChatGPT by OpenAI.

Author contributions

Daniel Polyakov (Conceptualization [Lead], Formal analysis [Lead], Investigation [Lead], Methodology [Lead], Project administration [Equal], Software [Lead], Validation [Lead], Visualization [Lead], Writing—original draft [Lead], Writing—review & editing [Lead]), P. A. Robinson (Methodology, Software, Writing—review & editing [Equal]), Avigail Makbili (Formal analysis, Software, Writing—review & editing [Supporting]), Steven Laureys (Data curation [Lead], Funding acquisition [Equal], Writing—review & editing [Supporting]), Olivia Gosseries (Data curation [Equal], Funding acquisition [Equal], Methodology [Supporting], Project administration [Supporting], Supervision [Supporting], Validation [Supporting], Visualization [Supporting], Writing—review & editing [Equal]), and Oren Shriki (Conceptualization [Supporting], Formal analysis [Supporting], Funding acquisition [Equal], Investigation [Supporting], Methodology [Supporting], Project administration [Equal], Resources [Lead], Supervision [Lead], Visualization [Supporting], Writing—review & editing [Equal])

Conflict of interest

None declared.

Funding

This work was supported by the University and University Hospital of Liège, the Belgian National Funds for Scientific Research (FRS-FNRS), the FNRS PDR project (T.0134.21), the ERA-Net FLAG-ERA JTC2021 project ModelDXConsciousness (the Human Brain Project Partnering Project), the DoC-Box project (HORIZON-MSCA-2022-SE-01-01-101131344), and the FNRS MIS project (F.4521.23).

Compliance with ethical standards

The study was approved by the ethical committee at the Medicine Faculty of the University of Liege, Belgium, in accordance with the Declaration of Helsinki. All healthy subjects gave written informed consent, while for non-communicating brain-injured patients, the informed consent was obtained from a legal surrogate.

Data availability

The data underlying this article will be shared on reasonable request to the corresponding author.

References

Abeysuriya RG, Robinson PA. Real-time automated EEG tracking of brain states using neural field theory. *J Neurosci Methods* 2016;**258**:28–45. https://doi.org/10.1016/j.jneumeth.2015.09.026

Abeysuriya RG, Rennie CJ, Robinson PA. Physiologically based arousal state estimation and dynamics. *J Neurosci Methods* 2015;**253**:55–69. https://doi.org/10.1016/j.jneumeth.2015.06.002

van Albada SJ, Robinson PA. Mean-field modeling of the basal ganglia-thalamocortical system. I. Firing rates in healthy and parkinsonian states. *J Theor Biol* 2009;**257**:642–63. https://doi.org/10.1016/j.jtbi.2008.12.018

Annen J, Frasso G, van der Lande GJ. *et al*. Cerebral electrometabolic coupling in disordered and normal states of consciousness. *Cell Rep* 2023;**42**:112854. https://doi.org/10.1016/j.celrep.2023.112854

Assadzadeh S, Annen J, Sanz L. *et al*. Method for quantifying arousal and consciousness in healthy states and severe brain injury via EEG-based measures of corticothalamic physiology. *J Neurosci Methods* 2023;**398**:109958. https://doi.org/10.1016/j.jneumeth.2023.109958

Bai Y, Lin Y, Ziemann U. Managing disorders of consciousness: the role of electroencephalography. *J Neurol* 2021;**268**:4033–65. https://doi.org/10.1007/s00415-020-10095-z

Bernat JL. Chronic disorders of consciousness. *Lancet Neurol* 2006;**14**:1277–83. https://doi.org/10.3892/etm.2017.4639

Bodien YG, Martens G, Ostrow J. *et al*. Cognitive impairment, clinical symptoms and functional disability in patients emerging from the minimally conscious state. *NeuroRehabilitation* 2020;**46**:65–74. https://doi.org/10.3233/NRE-192860

Boly M, Massimini M, Tsuchiya N. *et al*. Are the neural correlates of consciousness in the front or in the back of the cerebral cortex? Clinical and neuroimaging evidence. *J Neurosci* 2017;**37**:9603–13. https://doi.org/10.1523/JNEUROSCI.3218-16.2017

Braitenberg, V. and Schüz, A. *Cortex: Statistics and Geometry of Neuronal Connectivity*. Berlin: Springer, Berlin Heidelberg. 2 edn, 1998. https://doi.org/10.1007/978-3-662-03733-1

Breakspear M, Roberts JA, Terry JR. *et al*. A unifying explanation of primary generalized seizures through nonlinear brain modeling and bifurcation analysis. *Cereb Cortex* 2006;**16**:1296–313. https://doi.org/10.1093/cercor/bhj072

Brown EN, Lydic R, Schiff ND. General anesthesia, sleep, and coma. *N Engl J Med* 2010;**363**:2638–50. https://doi.org/10.1056/NEJMra0808281

Bruno MA, Vanhaudenhuyse A, Thibaut A. *et al*. From unresponsive wakefulness to minimally conscious PLUS and functional locked-in syndromes: recent advances in our understanding of disorders of consciousness. *J Neurol* 2011;**258**:1373–84. https://doi.org/10.1007/s00415-011-6114-x

Carrière M, Cassol H, Aubinet C. *et al*. Auditory localization should be considered as a sign of minimally conscious state based on multimodal findings. *Brain Commun* 2020;**2**:1–15. https://doi.org/10.1093/braincomms/fcaa195

Casali AG, Gosseries O, Rosanova M. *et al*. A theoretically based index of consciousness independent of sensory processing and behavior. *Sci Transl Med* 2013;**5**. https://doi.org/10.1126/scitranslmed.3006294

Colombo MA, Napolitani M, Boly M. *et al*. The spectral exponent of the resting EEG indexes the presence of consciousness during unresponsiveness induced by propofol, xenon, and ketamine. *NeuroImage* 2019;**189**:631–44. https://doi.org/10.1016/j.neuroimage.2019.01.024

Crick F, Koch C. Towards a neurobiological theory of consciousness. *Semin Neurosci* 1990;**25**:251–62. https://doi.org/10.3828/sj.2016.25.2.9

Darracq M, Funk CM, Polyakov D. *et al*. Evoked alpha power is reduced in disconnected consciousness during sleep and anesthesia. *Sci Rep* 2018;**8**:1–10. https://doi.org/10.1038/s41598-018-34957-9

Deco G, Jirsa VK, Robinson PA. *et al*. The dynamic brain: from spiking neurons to neural masses and cortical fields. *PLoS Comput Biol* 2008;**4**. https://doi.org/10.1371/journal.pcbi.1000092

Delorme A, Makeig S. EEGLAB: an open source toolbox for analysis of single-trial EEG dynamics including independent component analysis. *J Neurosci Methods* 2004;**134**:9–21. https://doi.org/10.1016/j.jneumeth.2003.10.009

Demertzi A, Tagliazucchi E, Dehaene S. *et al*. Human consciousness is supported by dynamic complex patterns of brain signal coordination. *Sci Adv* 2019;**5**:eaat7603–11. https://doi.org/10.1126/sciadv.aat7603

Donoghue T, Haller M, Peterson EJ. *et al*. Parameterizing neural power spectra into periodic and aperiodic components. *Nat Neurosci* 2020;**23**:1655–65. https://doi.org/10.1038/s41593-020-00744-x

Fekete T, Omer DB, O'Hashi K. *et al*. Critical dynamics, anesthesia and information integration: lessons from multi-scale criticality analysis of voltage imaging data. *NeuroImage* 2018;**183**:919–33. https://doi.org/10.1016/j.neuroimage.2018.08.026

Freeman WJ, Zhai J. Simulated power spectral density (PSD) of background electrocorticogram (ECoG). *Cogn Neurodyn* 2009;**3**:97–103. https://doi.org/10.1007/s11571-008-9064-y

Fulcher BD, Phillips AJ, Robinson PA. Modeling the impact of impulsive stimuli on sleep-wake dynamics. *Phys Rev E* 2008;**78**:1–14. https://doi.org/10.1103/PhysRevE.78.051920

Gao R, Peterson EJ, Voytek B. Inferring synaptic excitation/inhibition balance from field potentials. *NeuroImage* 2017;**158**:70–8. https://doi.org/10.1016/j.neuroimage.2017.06.078

Gervais C, Boucher LP, Villar GM. *et al*. A scoping review for building a criticality-based conceptual framework of altered states of consciousness. *Front Syst Neurosci* 2023;**17**. https://doi.org/10.3389/fnsys.2023.1085902

Giacino JT, Kalmar K, Whyte J. The JFK coma recovery scale-revised: measurement characteristics and diagnostic utility. *Arch Phys Med Rehabil* 2004;**85**:2020–9. https://doi.org/10.1016/j.apmr.2004.02.033

Gosseries O, Bruno MA, Chatelle C. *et al*. Disorders of consciousness: what's in a name? *NeuroRehabilitation* 2011;**28**:3–14. https://doi.org/10.3233/NRE-2011-0625

Groppe DM, Urbach TP, Kutas M. Mass univariate analysis of event-related brain potentials/fields I: a critical tutorial review. *Psychophysiology* 2011;**48**:1711–25. https://doi.org/10.1111/j.1469-8986.2011.01273.x

Haun AM, Oizumi M, Kovach CK. *et al*. Conscious perception as integrated information patterns in human electrocorticography. *eNeuro* 2017;**4**:ENEURO.0085–17.2017. https://doi.org/10.1523/ENEURO.0085-17.2017

Jansen BH, Rit VG. Electroencephalogram and visual evoked potential generation in a mathematical model of coupled cortical columns. *Biol Cybern* 1995;**73**:357–66. https://doi.org/10.1007/BF00199471

Kerr CC, Rennie CJ, Robinson PA. Physiology-based modeling of cortical auditory evoked potentials. *Biol Cybern* 2008;**98**:171–84. https://doi.org/10.1007/s00422-007-0201-1

Koch C, Tsuchiya N. Attention and consciousness: two distinct brain processes. *Trends Cogn Sci* 2007;**11**:16–22. https://doi.org/10.1016/j.tics.2006.10.012

Koch C, Massimini M, Boly M. *et al*. Neural correlates of consciousness: progress and problems. *Nat Rev Neurosci* 2016;**17**:307–21. https://doi.org/10.1038/nrn.2016.22

Lau H, Rosenthal D. Empirical support for higher-order theories of conscious awareness. *Trends Cogn Sci* 2011;**15**:365–73. https://doi.org/10.1016/j.tics.2011.05.009

Laufs H, Vuust P, Deco G. *et al*. Discovery of key whole-brain transitions and dynamics during human wakefulness and non-REM sleep. *Nat Commun* 2019;**10**:1–14. https://doi.org/10.1038/s41467-019-08934-3

Li D, Mashour GA. Cortical dynamics during psychedelic and anesthetized states induced by ketamine. *NeuroImage* 2019;**196**:32–40. https://doi.org/10.1016/j.neuroimage.2019.03.076

Li G, Liu Y, Zheng Y. *et al*. Multiscale neural modeling of resting-state fMRI reveals executive-limbic malfunction as a core mechanism in major depressive disorder. *NeuroImage Clin* 2021;**31**:102758. https://doi.org/10.1016/j.nicl.2021.102758

Markram H. The Blue Brain Project. *Nat Rev Neurosci* 2006;**7**:153–60. https://doi.org/10.1038/nrn1848

Martens G, Ibáñez-Soria D, Barra A. *et al*. A novel closed-loop EEG-tDCS approach to promote responsiveness of patients in minimally conscious state: a study protocol. *Behav Brain Res* 2021;**409**:113311. https://doi.org/10.1016/j.bbr.2021.113311

Maschke C, Duclos C, Owen AM. *et al*. Aperiodic brain activity and response to anesthesia vary in disorders of consciousness. *Neuroimage* 2023;**275**:120154. https://doi.org/10.1016/j.neuroimage.2023.120154

Mashour GA, Hudetz AG. Neural correlates of unconsciousness in large-scale brain networks. *Trends Neurosciences* 2018;**41**:150–60. https://doi.org/10.1016/j.tins.2018.01.003

Mateos DM, Guevara Erra R, Wennberg R. *et al*. Measures of entropy and complexity in altered states of consciousness. *Cogn Neurodyn* 2018;**12**:73–84. https://doi.org/10.1007/s11571-017-9459-8

Medel V, Irani M, Crossley N. *et al*. Complexity and 1/f slope jointly reflect brain states. *Sci Rep* 2023;**13**:21700–12. https://doi.org/10.1038/s41598-023-47316-0

Mohanta S, Afrasiabi M, Casey CP. *et al*. Predictive feedback, early sensory representations, and fast responses to predicted stimuli depend on NMDA receptors. *J Neurosci* 2021;**41**:10130–47. https://doi.org/10.1523/jneurosci.1311-21.2021

Müller EJ, van Albada SJ, Kim JW. *et al*. Unified neural field theory of brain dynamics underlying oscillations in Parkinson's disease and generalized epilepsies. *J Theor Biol* 2017;**428**:132–46. https://doi.org/10.1016/j.jtbi.2017.06.016

Muller EJ, Munn BR, Redinbaugh MJ. *et al*. The non-specific matrix thalamus facilitates the cortical information processing modes relevant for conscious awareness. *Cell Rep* 2023;**42**:112844. https://doi.org/10.1016/j.celrep.2023.112844

Nevado-Holgado AJ, Marten F, Richardson MP. *et al*. Characterising the dynamics of EEG waveforms as the path through parameter space of a neural mass model: application to epilepsy seizure evolution. *NeuroImage* 2012;**59**:2374–92. https://doi.org/10.1016/j.neuroimage.2011.08.111

Nunez PL. *Neocortical Dynamics and Human EEG Rhythms*. New York, NY, USA: Oxford University Press, 1995.

O'Connor SC, Robinson PA. Spatially uniform and nonuniform analyses of electroencephalographic dynamics, with application to the topography of the alpha rhythm. *Phys Rev E* 2004;**70**:19. https://doi.org/10.1103/PhysRevE.70.011911

O'Connor SC, Robinson PA. Analysis of the electroencephalographic activity associated with thalamic tumors. *J Theor Biol* 2005;**233**:271–86. https://doi.org/10.1016/j.jtbi.2004.10.009

Ouyang G, Li J, Liu X. *et al*. Dynamic characteristics of absence EEG recordings with multiscale analysispermutation entropy. *Epilepsy Res* 2013;**104**:246–52. https://doi.org/10.1016/j.eplepsyres.2012.11.003

Pal D, Li D, Dean JG. *et al*. Level of consciousness is dissociable from electroencephalographic measures of cortical connectivity, slow oscillations, and complexity. *J Neurosci* 2019;**40**:605–18. https://doi.org/10.1523/JNEUROSCI.1910-19.2019

Penfield, W. and Jasper, H. *Epilepsy and the Functional Anatomy of the Human Brain*. Boston: Brown. Vol. **47**, 704, 1954. https://doi.org/10.1097/00007611-195407000-00024

Piarulli A, Bergamasco M, Thibaut A. *et al*. EEG ultradian rhythmicity differences in disorders of consciousness during wakefulness. *J Neurol* 2016;**263**:1746–60. https://doi.org/10.1007/s00415-016-8196-y

Pion-Tonachini L, Kreutz-Delgado K, Makeig S. ICLabel: an automated electroencephalographic independent component classifier, dataset, and website. *Neuroimage* 2019;**198**:181–97. https://doi.org/10.1016/j.neuroimage.2019.05.026

Polyakov D, Robinson PA, Muller EJ. *et al*. Personalized stimulation therapies for disorders of consciousness: a computational approach to inducing healthy-like brain activity based on neural field theory. *J Neural Eng* 2025;**22**:1–24. https://doi.org/10.1088/1741-2552/addd48

Rennie CJ, Robinson PA, Wright JJ. Unified neurophysical model of EEG spectra and evoked potentials. *Biol Cybern* 2002;**86**:457–71. https://doi.org/10.1007/s00422-002-0310-9

Robinson PA. The balanced and introspective brain. *J R Soc Interface* 2017;**14**:1–7. https://doi.org/10.1098/rsif.2016.0994

Robinson PA. Physical brain connectomics. *Phys Rev E* 2019;**99**:23–5. https://doi.org/10.1103/PhysRevE.99.012421

Robinson PA. Neural field theory of neural avalanche exponents. *Biol Cybern* 2021;**115**:237–43. https://doi.org/10.1007/s00422-021-00875-9

Robinson PA, Rennie CJ, Wright JJ. Propagation and stability of waves of electrical activity in the cerebral cortex. *Phys Rev E* 1997;**56**:826–40. https://doi.org/10.1103/physreve.56.826

Robinson PA, Rennie CJ, Wright JJ. *et al*. Prediction of electroencephalographic spectra from neurophysiology. *Phys Rev E* 2001;**63**:0219031–02190318. https://doi.org/10.1103/PhysRevE.63.021903

Robinson PA, Rennie CJ, Rowe DL. Dynamics of large-scale brain activity in normal arousal states and epileptic seizures. *Phys Rev E* 2002;**65**:9. https://doi.org/10.1103/PhysRevE.65.041924

Robinson PA, Rennie CJ, Rowe DL. *et al*. Estimation of multiscale neurophysiologic parameters by electroencephalographic means. *Hum Brain Mapp* 2004;**23**:53–72. https://doi.org/10.1002/hbm.20032

Robinson PA, Rennie CJ, Rowe DL. *et al*. Multiscale brain modelling. *Phil Trans R Soc B Biol Sci* 2005;**360**:1043–50. https://doi.org/10.1098/rstb.2005.1638

Robinson PA, Phillips AJ, Fulcher BD. *et al*. Quantitative modelling of sleep dynamics. *Philos Trans R Soc A Math Phys Eng Sci* 2011;**369**:3840–54. https://doi.org/10.1098/rsta.2011.0120

Robinson PA, Sarkar S, Pandejee GM. *et al*. Determination of effective brain connectivity from functional connectivity with application to resting state connectivities. *Phys Rev E* 2014;**90**:1–6. https://doi.org/10.1103/PhysRevE.90.012707

Rowe DL, Robinson PA, Rennie CJ. Estimation of neurophysiological parameters from the waking EEG using a biophysical model of brain dynamics. *J Theor Biol* 2004;**231**:413–33. https://doi.org/10.1016/j.jtbi.2004.07.004

Sanchez-Vives MV, Massimini M, Mattia M. Shaping the default activity pattern of the cortical network. *Neuron* 2017;**94**:993–1001. https://doi.org/10.1016/j.neuron.2017.05.015

Sanz-Leon P, Knock SA, Woodman MM. *et al*. The virtual brain: a simulator of primate brain network dynamics. *Front Neuroinform* 2013;**7**. https://doi.org/10.3389/fninf.2013.00010

Sanz-Leon P, Robinson PA, Knock SA. *et al*. NFTsim: theory and simulation of multiscale neural field dynamics. *PLoS Comput Biol* 2018;**14**:e1006387–37. https://doi.org/10.1371/journal.pcbi.1006387

Schartner MM, Carhart-harris RL, Barrett AB, Seth AK. Increased spontaneous MEG signal diversity for psychoactive doses of ketamine, *LSD and Psilocybin*. *Sci Rep* 2017;**7**:46421. https://doi.org/10.1038/srep46421

Sergent C, Corazzol M, Labouret G. *et al*. Bifurcation in brain dynamics reveals a signature of conscious processing independent of report. *Nat Commun* 2021;**12**:1149. https://doi.org/10.1038/s41467-021-21393-z

Shriki O, Yellin D. Optimal information representation and criticality in an adaptive sensory recurrent neuronal network. *PLoS Comput Biol* 2016;**12**:e1004698–19. https://doi.org/10.1371/journal.pcbi.1004698

Thibaut A, Panda R, Annen J. *et al*. Preservation of brain activity in unresponsive patients identifies MCS star. *Ann Neurol* 2021;**90**:89–100. https://doi.org/10.1002/ana.26095

Tononi G. Consciousness as integrated information: a provisional manifesto. *Biol Bull* 2008;**215**:216–42. https://doi.org/10.2307/25470707

Tononi G, Boly M, Gosseries O. *et al*. *The Neurology of Consciousness: An Overview*. 2nd edn. Elsevier Ltd, 2016a.

Tononi G, Boly M, Massimini M. *et al*. Integrated information theory: from consciousness to its physical substrate. *Nat Rev Neurosci* 2016b;**17**:450–61. https://doi.org/10.1038/nrn.2016.44

Vanhaudenhuyse A, Noirhomme Q, Tshibanda LJ. *et al*. Default network connectivity reflects the level of consciousness in non-communicative brain-damaged patients. *Brain* 2010;**133**:161–71. https://doi.org/10.1093/brain/awp313

Wang HE, Triebkorn P, Breyton M. *et al*. Virtual brain twins: from basic neuroscience to clinical use. *Natl Sci Rev* 2024;**11**. https://doi.org/10.1093/nsr/nwae079

Whyte CJ, Redinbaugh MJ, Shine JM. *et al*. Thalamic contributions to the state and contents of consciousness. *Neuron* 2024;**112**:1611–25. https://doi.org/10.1016/j.neuron.2024.04.019

Wilson HR, Cowan JD. A mathematical theory of the functional dynamics of cortical and thalamic nervous tissue. *Kybernetik* 1973;**13**:55–80. https://doi.org/10.1007/BF00288786

Neuroscience of Consciousness, 2025, **2025(1)**, **2025**, niaf055
https://doi.org/10.1093/nconsc/niaf055
Research Article